

Optical properties of atmospheric fine particles near Beijing during the HOPE-J³A Campaign

Xuezhe Xu^{1,2,3}, Weixiong Zhao^{1,2}, Qilei Zhang^{1,2,3}, Shuo Wang^{1,2,3}, Bo Fang^{1,2}, Weidong Chen⁵, Dean S. Venables^{6,7}, Xinfeng Wang⁸, Wei Pu⁹, Xin Wang⁹, Xiaoming Gao^{1,2,4}, and Weijun Zhang^{1,2,4}

¹ Key Laboratory of Atmospheric Composition and Optical Radiation, Anhui Institute of Optics and Fine Mechanics, Chinese Academy of Sciences, Hefei 230031, Anhui, China

² Laboratory of Atmospheric Physico-Chemistry, Anhui Institute of Optics and Fine Mechanics, Chinese Academy of Sciences, Hefei, 230031, Anhui, China

³ Graduate School, University of Science and Technology of China, Hefei, 230026, Anhui, China

⁴ School of Environmental Science and Optoelectronic Technology, University of Science and Technology of China, Hefei, 230026, Anhui, China

⁵ Laboratoire de Physicochimie de l'Atmosphère, Université du Littoral Côte d'Opale, 59140 Dunkerque, France

⁶ Department of Chemistry and Environmental Research Institute, University College Cork, Cork, Ireland

⁷ Leibniz Institute for Tropospheric Research, 04318 Leipzig, Germany

⁸ Environment Research Institute, Shandong University, Jinan 250100, China

⁹ Key Laboratory for Semi-Arid Climate Change of the Ministry of Education, College of Atmospheric Sciences, Lanzhou University, Lanzhou 730000, China

*Correspondence to :

Weixiong Zhao (wxzhao@aiofm.ac.cn) and Weijun Zhang (wjzhang@aiofm.ac.cn)

1 **Abstract**

2 The optical properties and chemical composition of PM_{1.0} particles in a suburban environment
3 (Huairou) near the mega-city of Beijing were measured during the HOPE-J³A (Haze Observation
4 Project Especially for Jing-Jin-Ji Area) field campaign. The campaign covered the period November
5 2014 to January 2015 during the winter coal heating season. The average values and standard
6 deviations of the extinction, scattering, absorption coefficients, and the aerosol single scattering
7 albedo (SSA) at $\lambda = 470$ nm during the measurement period were 201 ± 240 , 164 ± 202 , 37 ± 43
8 Mm^{-1} , and 0.80 ± 0.08 , respectively. The average values for the real and imaginary components of
9 the effective complex refractive index (CRI) over the campaign were 1.40 ± 0.06 and 0.03 ± 0.02 ,
10 while the average mass scattering and absorption efficiencies (MSE and MAE) of PM_{1.0} were 3.6 and
11 $0.7 \text{ m}^2 \text{ g}^{-1}$, respectively. Highly time-resolved air pollution episodes clearly show the dramatic
12 evolution of the PM_{1.0} size distribution, extensive optical properties (extinction, scattering, and
13 absorption coefficients) and intensive optical properties (single scattering albedo and CRI) during
14 haze formation, development and decline. Time periods were classified into three different pollution
15 levels (clear, slightly polluted, and polluted) for further analysis. It was found that: (1) The relative
16 contributions of organic and inorganic species to observed aerosol composition changed significantly
17 from clear to polluted days: the organic mass fraction decreased from 50% to 43% while the
18 proportion of sulfates, nitrates, and ammonium increased strongly from 34% to 44%. (2) Chemical
19 apportionment of extinction, calculated using the IMPROVE algorithm, tended to underestimate the
20 extinction compared to measurements. Agreement with measurements was improved by modifying
21 the parameters to account for enhanced absorption by elemental carbon (EC). Organic mass was the
22 largest contributor (52%) to the total extinction of PM_{1.0}, while EC, despite its low mass
23 concentration of ca. 4%, contributed about 17%, to extinction. When the air quality deteriorated, the
24 contribution of nitrate aerosol increased significantly (from 15% on clear days to 22% on polluted
25 days). (3) Under polluted conditions, the average mass absorption efficiencies (MAE) of EC were up
26 to 4 times as large as the reference MAE value for freshly generated black carbon (BC). The
27 temporal pattern of MAE values was similar to that of the OC/EC ratio, suggesting that non-BC
28 absorption from secondary organic aerosol (SOA) also contributes to particle absorption.

29

30

1 **1 Introduction**

2

3 Atmospheric aerosols have significant effects on climate forcing (Ramanathan et al., 2001;
4 Anderson et al., 2003; Wang et al., 2010; Bahadur et al., 2012), environment (Cao et al., 2013;
5 Huang et al., 2014), and human health (Nel, 2005; S. Zheng et al., 2015). Visibility is regarded as an
6 indicator of air quality and is affected by the scattering and absorption of solar light by fine particles
7 (Watson, 2002). Uncertainties in atmospheric visibility are mainly due to the uncertainties associated
8 with the aerosols' optical properties, which depend on the physical and chemical properties of
9 atmospheric aerosol, including chemical composition, size distribution, mixing state, morphology
10 and hygroscopic properties. Understanding how these physical and chemical characteristics affect the
11 optical properties of particles is key to improve quantitative estimates of direct radiative forcing and
12 to determine the environmental effects of particles. To ascertain the relationships between these
13 parameters, many research campaigns have been performed during the past decade, including ACE-1
14 (Bates et al., 1998), ACE-2 (Raes et al., 2000), INDOEX (Eldering, 2002), ACE-Asia (Quinn, 2004;
15 Doherty et al., 2005), PRIDE-PRD2004 (Zhang et al., 2008), MILAGRO (Marley et al., 2009),
16 CAREBeijing (Jung et al., 2009; Garland et al., 2009; Wu et al., 2011) and CalNex campaign (Cahill
17 et al., 2012; Thompson et al., 2012; Ryerson et al., 2013; X. Zhang et al., 2013).

18 Rapid urbanization and economic development has brought about serious environmental
19 problems in the megacities of China (L. Han et al., 2015). The North China Plain (NCP) region in
20 northeast China has one of the highest global aerosol concentrations (Sun et al., 2013) due to the
21 dense population, the large number of vehicles, and intense industrial activity. The China National
22 Ambient Air Quality Standard designates a daily average concentration of $PM_{2.5}$ greater than $75 \mu g$
23 m^{-3} as harmful to health. However, $PM_{2.5}$ concentrations in China often grossly exceed this limit –
24 for instance, daily average mass concentration of $PM_{2.5}$ in January 2013 were higher than $500 \mu g m^{-3}$
25 for Beijing (Andersson et al., 2015). A large amount of atmospheric pollutants are emitted from
26 fossil fuel, biomass burning and urban construction (Lei et al., 2011; Zhang et al., 2011). The
27 mixture of these various emissions results in complex physical, chemical and optical properties of
28 aerosols in the NCP region.

29 In recent years, many campaigns have been conducted in Beijing (Liu et al., 2013; Sun et al.,
30 2013, 2015; Guo et al., 2014; Andersson et al., 2015; B. Han et al., 2015; Wang et al., 2015; Wu et

1 al., 2015; Xu et al., 2011; X. J. Zhao et al., 2013; G. J. Zheng et al., 2015). It is worth noting that
2 atmospheric dynamic processes differ between polluted and cleaner periods and that secondary
3 aerosols have been proposed as the major contributor to haze formation (Quan et al., 2014; Sun et al.,
4 2014). Research in the Pearl River Delta of China has shown that submicron particles contribute
5 more than 90% of the particle extinction (Cheng et al., 2008). However, few studies in the NCP
6 region have focused on the contribution of submicron aerosol to light extinction under different air
7 pollution conditions. Moreover, the evolution of intensive optical properties (effective complex
8 refractive index, CRI, and single scattering albedo, SSA or ω , the ratio of scattering to extinction) in
9 haze formation, development and decline have rarely been reported. Comprehensive studies of
10 intensive optical properties and light apportionment are necessary for a better understanding of the
11 evolution of aerosol physical and optical properties in the NCP.

12 In this paper, we report continuous measurements of the optical properties, particle size
13 distributions, and chemical composition of submicron aerosol at a suburban site (Huairou) from 16
14 November 2014 to 11 January 2015. The effective CRI for $PM_{1.0}$ particles were retrieved with Mie
15 theory by treating the submicron aerosols as spherical particles. The fractional contribution of the
16 chemical components of particles to the total extinction coefficient were calculated by the modified
17 IMPROVE algorithm (Pitchford et al., 2007). $PM_{1.0}$ optical properties, chemical compositions, size
18 distributions, chemical apportionment of light extinction, and mass scattering and absorption
19 efficiencies are reported for three different pollution levels.

20 21 **2 Experimental**

22
23 The Haze Observation Project Especially for Jing-Jin-Ji (Beijing-Tianjin-Hebei, the national
24 capital region of China) Area (HOPE-J³A) field campaign took place at the Huairou campus of the
25 University of Chinese Academy of Sciences (40°24'24.45"N, 116°40'32.95"E) from October 2014 to
26 January 2015. The goal of the HOPE-J³A campaign was to better understand the emissions, transport,
27 and evolution of atmospheric fine particles and their precursors in the Jing-Jin-Ji area. Figure 1
28 shows the map of NCP and the average distribution of the MODIS (MODerate-resolution Imaging
29 Spectroradiometer) (Chu et al., 2003) AOD (aerosol optical depth) with a resolution of 0.2°×0.2°
30 during the field campaign from 16 November 2014 to 11 January 2015. The Huairou observation site

1 (marked as a red star in Fig. 1) is situated about 60 km northeast of Beijing city center and is mainly
2 surrounded by medium density residential suburban areas.

3 The instruments were installed on the 4th floor of Teaching Building 1, with the sample inlet
4 about 2.5 m above the roof. The inlet consisted of a PM_{1.0} ambient size cut (SF-PM_{1.0}, 1.0 m³ h⁻¹,
5 Sven Leckel Ingenieurburo GmbH) with a 50% cut-point at 1.0 μm. Downstream of the inlet, the
6 sample air was dried to below 15% RH by a diffusion dryer and then passed through a copper tube (6
7 m long with an inner diameter of 1 cm) at a flow rate of 16.7 L min⁻¹.

8 The particle size distribution between 14 and 662 nm was measured every 3 min with a scanning
9 mobility particle sizer (SMPS, TSI 3936), which comprised an electrostatic classifier (TSI 3080) and
10 a condensation particle counter (TSI 3776). Diffusion losses and the effect of multicharged particles
11 were corrected by the instrument software. The SMPS was validated with laboratory-generated,
12 NIST traceable monodispersed polystyrene latex (PSL) spheres with diameters of 203 ± 5 nm
13 (Thermo Scientific 3200A) and 296 ± 6 nm (Thermo Scientific 3300A) before and after the
14 campaign (W. Zhao et al., 2013). The measured particle sizes and the certified diameters of the PSL
15 spheres agreed to within 2 %.

16 The optical properties of PM_{1.0} particles were measured with a newly developed cavity-enhanced
17 albedometer (Zhao et al., 2014a). The albedometer was based on a blue light-emitting-diode (LED)
18 incoherent broadband cavity-enhanced absorption spectroscopy (IBBCEAS) system that
19 incorporated an integrating sphere (IS). This instrument is a new tool for direct, in situ, and
20 simultaneous measurement of aerosol scattering and extinction coefficients (and thus of the
21 absorption coefficient and aerosol SSA, ω_{470}) at a mean wavelength of 470 nm. The performance of
22 the cavity-enhanced albedometer was previously evaluated using laboratory-generated, monodisperse
23 standard aerosol particles, and the scattering measurements were also found to be in close agreement
24 with TSI 3563 nephelometer measurements (Zhao et al., 2014 a, b).

25 The advantage of broadband over single wavelength measurements is its capacity to
26 simultaneously measure multiple species present in the sample (gases and particles) using a single
27 instrument. A spectral-fitting algorithm was applied from 445 to 480 nm to retrieve gas
28 concentrations based on their spectral structure and thereby to remove the contribution of gas phase
29 absorption from the aerosol extinction. The scattering signal in the IS was measured by a single
30 channel photomultiplier tube (PMT), providing an integrated result over a narrow bandwidth of ~ 9

1 nm (full-width at half maximum, FWHM) in the spectral region of 465–474 nm. Truncation
2 reduction tubes (Varma et al., 2003) were used to minimize the forward and backward truncation
3 angles to 1.2°.

4 The sample volume of the system was about 1.8 L and the flow rate of the cavity-enhanced
5 albedometer was 1.5 L min⁻¹ at atmospheric pressure. The acquisition time for each measurement
6 was 9 s (for a 1.5 s integrating time per spectrum, and six-spectra averaging). The temperature and
7 relative humidity of the sample were measured with a hygrometer (Rotronic, model HC2 humidity
8 sensor). The cavity was flushed with dry zero air every hour to acquire a reference spectrum. The
9 reference spectrum was used both in the IBBCEAS retrieval (Fiedler et al., 2003) and to remove the
10 contribution of light scattering from internal surfaces and Rayleigh scattering. The mirror reflectivity
11 $R(\lambda)$ and the scaling factor (K' , the calibration coefficient that related instrument response to
12 scattering magnitude) for the scattering channel of the albedometer were determined by He, N₂ and
13 CO₂ every week. No deterioration of R and K' were observed during the campaign.

14 The detection limits for the scattering and extinction channels with 9 s integration time were
15 0.54 Mm⁻¹ and 0.15 Mm⁻¹, respectively. The total uncertainty in the extinction measurement was
16 estimated to be less than 4% and arose from uncertainties in the mirror reflectivity (R) (~1%), the
17 ratio of cavity length to the cell length containing the air sample when the cavity mirrors were purged
18 (R_L) (~3%), and particle losses in the system (~2%). The total uncertainty in the scattering
19 measurement was about 3%, with dominant contributions from uncertainties in the experimentally
20 determined scattering calibration coefficient (K') (2%), and the uncertainty associated with particle
21 losses in the cavity (2%).

22 Based on a Mie scattering calculation, the truncated fraction of total scattering was about 0.22%
23 for a 1 μm diameter spherical particle with a complex refractive index (CRI) of $m = 1.6 + i0$ at $\lambda =$
24 470 nm. This truncation effect was therefore negligible compared to the measurement uncertainty
25 and no correction for the truncation underestimate was applied to our data.

26 Potential uncertainties associated with changes in the instrument environment were considered
27 but found to be unimportant. The instrument was located in a temperature-controlled room, the
28 temperature inside the albedometer enclosure was maintained at $28.3 \pm 0.8^\circ\text{C}$, and the sample flow
29 was controlled with a mass flow meter. Example data of the transmitted intensity measured with the
30 CCD spectrometer and the scattering signal measured with the PMT are shown in Fig. S1. The cavity

1 was flushed with particle-free air every hour to acquire the $I_0(\lambda)$ spectrum. No obvious drift in the
2 LED light intensity was observed even after 6 hours of measurement, indicating the high stability of
3 the instrument under these operating conditions.

4 Another $PM_{1.0}$ sampler (SF- $PM_{1.0}$, Sven Leckel Ingenieurburo GmbH) was installed on the roof
5 of the building (~ 20 m above the ground) to collect $PM_{1.0}$ samples with quartz filters (47 mm,
6 MUNKTELL Corporation) for off-line aerosol chemical composition analysis. The flow rate was
7 16.7 L min^{-1} and samples were collected over the period of 16 November 2014 to 11 January 2015.
8 The collection time period was 12 h: from 08:30 to 20:30 LT for daytime samples, and from 20:30 to
9 08:30 LT for nighttime samples. Before sampling, the quartz-fiber filters were preheated for 4 h at
10 600°C in a muffle furnace, and ten filters were used as field blank samples in the sampling period. In
11 total, 114 filters were collected; these were stored at -4°C to prevent evaporation of volatilized
12 species until they were analyzed.

13 A punch of 1.5 cm^2 was taken from each filter and then heated in inert and oxidizing
14 atmospheres to volatilize and combust the loaded carbon, respectively. The carbon (elemental carbon,
15 EC, and organic carbon, OC) concentrations were determined with a thermal/optical transmittance
16 aerosol carbon analyzer (Sunset Laboratory, Inc.) (NIOSH, 1996). The measurement principle and
17 operation of the Sunset aerosol carbon analyzer was presented in a previous study (Peterson et al.,
18 2002). Another punch with a area of 2 cm^2 was taken from the rest of filter, extracted into 10 mL of
19 deionized water ($> 18\text{M}\Omega$) via 20 min sonication, filtered using a $0.22 \mu\text{m}$ PTFE syringe filter, and
20 stored in a refrigerator at 4°C until chemical analysis. Eight water-soluble ion compositions [three
21 anions: nitrate (NO_3^-), sulfate (SO_4^{2-}), and chloride (Cl^-); five cations: ammonium (NH_4^+), sodium
22 (Na^+), potassium (K^+), magnesium (Mg^{2+}) and calcium (Ca^{2+})] were determined using a Dionex
23 ICS-90 Ion Chromatography system with AS14A and CS14A columns and eluents of
24 $\text{NaCO}_3\text{-NaHCO}_3$ and methanesulfonic acid, respectively. Further details on this analysis are given
25 elsewhere (X. F. Wang et al., 2013).

26 Meteorological parameters, including wind speed (WS) and direction (WD), temperature (T) and
27 relative humidity (RH), were continuously recorded at the observation site. The mass concentration
28 of $PM_{2.5}$ for the air quality classification and concentrations of pollutant gases (SO_2 , NO_2 , O_3 , and
29 CO) were monitored by the National Environmental Bureau and the data at Huairou were retrieved
30 from the internet (<http://113.108.142.147:20035/emcpublish/>). In this work, the $PM_{2.5}$ pollution level

1 was divided into three categories according to the technical regulation on Ambient Air Quality Index
 2 (National Environmental Protection Standard of the People's Republic of China, HJ 633–2012)
 3 (http://kjs.mep.gov.cn/hjbhzbz/bzwb/dqhbh/jcg_fbz/201203/W020120410332725219541.pdf; A.
 4 Zhang et al., 2013; G. J. Zheng et al., 2015): clear day ($PM_{2.5}$ concentration $\leq 35 \mu\text{g m}^{-3}$, when the
 5 corresponding individual air quality index (IAQI) of 24 hours averaged $PM_{2.5}$ concentration ranged
 6 from 0 to 50), slightly polluted day ($35 \mu\text{g m}^{-3} < PM_{2.5}$ concentration $\leq 115 \mu\text{g m}^{-3}$, when IAQI of
 7 $PM_{2.5}$ ranged from 50 to 150), and polluted day ($115 \mu\text{g m}^{-3} < PM_{2.5}$ concentration $\leq 350 \mu\text{g m}^{-3}$,
 8 when IAQI of $PM_{2.5}$ ranged from 150 to 400). These pollution classes are usually based on $PM_{2.5}$
 9 concentrations averaged from 00:00 to 23:59 on a specific date. For our filter samples, however, the
 10 collection time extended over two days; nevertheless, we applied the same categorization for our
 11 measurements from 20:30 (day 1) to 20:30 LT (day 2).

13 3 Optical data analysis method

15 3.1 Retrieval of aerosol complex refractive index

17 The scattering and extinction coefficients of particles are calculated based on (Pettersson et al.,
 18 2004):

$$19 \quad \alpha_{ep,sp} = \int N(D_p) \frac{\pi}{4} D_p^2 Q_{ext,scat}(m, x) dD_p \quad (1)$$

20 where $x = \pi D_p / \lambda$ is the size parameter, $m = n + i k$ is the CRI of the particle (where n and k
 21 correspond to the real and imaginary parts of the CRI, respectively), N is the number of particles per
 22 unit volume in the size bin dD_p with mean diameter D_p , and $\frac{\pi}{4} D_p^2 Q_{ext,scat}(m, x)$ is the extinction or
 23 scattering cross section $\sigma_{ep,sp}$. The extinction or scattering efficiency, $Q_{ext,scat}$, is a function of the CRI,
 24 the morphology of the particles and the size parameter. For chemically homogeneous spherical
 25 particles, Q can be calculated from Mie theory.

26 The effective CRI is an effective property that averages over the aerosols' size, shape, mixing
 27 state and chemical composition. Simultaneous measurement of the scattering and extinction

1 coefficients by the cavity-enhanced albedometer provides a new approach for faster retrieval of the
 2 particulate CRI (Riziq et al., 2007; Mack et al., 2010; Zhao et al., 2014a; Xu et al., 2016). Details of
 3 the CRI retrieval have been given in previous studies (Riziq et al., 2007; Mack et al., 2010). The
 4 measured extinction and scattering coefficients ($\alpha_{ep,470}$ and $\alpha_{sp,470}$) and the particle number size
 5 distribution, $N(D_p)$, were used to determine the effective CRI on the assumption that particles were
 6 spherical and that the black carbon aerosol (BC) can be treated in a volume mixing approach. The
 7 real and imaginary parts of the effective CRI were varied (between 1.3 and 1.7 for the real part and
 8 between 0 and 0.1 for the imaginary part) to calculate the extinction and scattering coefficients for
 9 each size distribution. A set of refractive indices were determined by finding the minimum of the
 10 “merit function”, χ^2 (Mack et al., 2010):

$$\chi^2 = \frac{(\alpha_{ep} - \alpha_{ep_calc})^2}{\varepsilon_{\alpha_{ep}}^2} + \frac{(\alpha_{sp} - \alpha_{sp_calc})^2}{\varepsilon_{\alpha_{sp}}^2} \quad (2)$$

12 Here, α_{ep} and α_{sp} are the measured values of the extinction and scattering coefficients, while α_{ep_calc}
 13 and α_{sp_calc} are the corresponding calculated values. $\varepsilon_{\alpha_{ep}}$ and $\varepsilon_{\alpha_{sp}}$ are the measurement uncertainty of
 14 α_{ep} and α_{sp} , respectively. The mean standard deviations of the extinction and scattering coefficients
 15 over 3 min were taken as the measurement uncertainty for calculating χ^2 .

16 A contour plot of χ^2 versus n and k was used to estimate the standard errors of n and k . The
 17 values of n and k that satisfied $\chi^2 < \chi_0^2 + 2.298$, which fell within the 1σ error bound of the best
 18 measurement (with 68% confidence level of χ^2 distribution), were considered acceptable. Projections
 19 of the contour lines (with a contour value of 2.298) on the n and k plane gave the standard errors Δn
 20 and Δk , respectively (Dinar et al., 2008; Zhao et al., 2014a).

21

22 3.2 Mass scattering and absorption efficiencies

23

24 Mass scattering (MSE) and absorption (MAE) efficiencies are the key parameters in climate and
 25 chemical transport models for estimating radiative forcing and apportioning chemical extinction
 26 budgets (Bates et al., 2006; Malm and Hand, 2007). MSE and MAE (both conventionally in units of
 27 $\text{m}^2 \text{g}^{-1}$) are defined as the ratio of the light scattering and absorption coefficients (Mm^{-1}) to the
 28 aerosol volume mass concentration ($\mu\text{g m}^{-3}$), respectively.

$$\text{MSE (MAE)} = \frac{\alpha_{\text{scat,abs}}}{M} \quad (3)$$

Knowledge of the MSEs and MAEs of each component of atmospheric aerosol is helpful for accurate source apportionment and for estimating radiative forcing in climate modes. The simplest method for computing MSE is by direct measurement of aerosol scattering coefficient and the mass concentration. The average MSE is estimated either by dividing the average α_{scat} by the average mass concentration or from the slope of a linear regression of α_{scat} and M (Hand and Malm, 2007). The MAE is calculated similarly.

In this study, the MSEs and MAEs of $\text{PM}_{1.0}$ were estimated from the slope of a linear regression of $\alpha_{\text{scat,abs}}$ and M (each data point with 3 min time resolution). The $\alpha_{\text{scat,abs}}$ was directly measured with the cavity-enhanced albedometer with high time resolution, and M was calculated from the average density ($\bar{\rho}$) and the volume concentrations ($V(D_p)$) measured with the SMPS ($M = \bar{\rho} \int V(D_p) dD_p$). The average density was calculated from $\bar{\rho}^{-1} = \sum_j \rho_j^{-1} X_j$, where ρ_j is the density of each chemical component (see Table S1), X_j is the mass concentration ratio of each species to the total $\text{PM}_{1.0}$ concentration (reconstructed with equation (S8)) measured from filter samples with a time resolution of 12 h sample⁻¹. If it is assumed that only EC contributes to aerosol absorption, the MAE of EC can be determined (Knox et al., 2009; Bond et al., 2013; Cheng et al., 2011, 2016):

$$\text{MAE} = \frac{\int_{t_1}^{t_2} \alpha_{\text{abs}} dt}{\text{EC}_m \times (t_2 - t_1)} \quad (4)$$

where EC_m ($\mu\text{g m}^{-3}$) is the measured EC mass concentration with the aerosol carbon analyzer, and t_1 and t_2 are the start and stop times for the collection of samples with quartz filters. In this work, the integration time was determined by the quartz filter sampling period of 12 h sample⁻¹. For comparison, the MAE of freshly generated BC is $8.7 \text{ m}^2 \text{ g}^{-1}$ at $\lambda = 470 \text{ nm}$ (based on a $7.5 \pm 1.2 \text{ m}^2 \text{ g}^{-1}$ at $\lambda = 550 \text{ nm}$ and using the inverse wavelength dependence) (Bond et al., 2006).

3.3 Chemical apportionment of aerosol optical properties

Chemical apportionment of light extinction of $PM_{1.0}$ was determined with a revised IMPROVE (Interagency Monitoring of Protected Visual Environments) algorithm (Pitchford et al., 2007). Although the IMPROVE algorithm is a simplified predictor of extinction, it is nevertheless a useful tool to estimate the contribution of different particle components to haze levels (Pitchford et al., 2007). In this study, the optical properties were measured at $\lambda = 470$ nm. The modified IMPROVE function for dry $PM_{1.0}$ extinction can be rewritten as following (with further details in the Supplement, Section S2.):

$$\begin{aligned} \alpha_{ext,470nm,PM_{1.0}} \approx & 2.88 \times [\text{Small Sulfate}] + 6.29 \times [\text{Large Sulfate}] \\ & + 3.14 \times [\text{Small Nitrate}] + 6.68 \times [\text{Large Nitrate}] \\ & + 3.64 \times [\text{Small Organic Mass}] + 7.93 \times [\text{Large Organic Mass}] \\ & + 10.8 \times [\text{Elemental Carbon}] + 2.23 \times [\text{Sea Salt}] \end{aligned} \quad (5)$$

The large and small parts are defined by the IMPROVE formula as (Pitchford et al., 2007; Cao et al., 2012):

$$[\text{Large X}] = [\text{Total X}]^2/20, \text{ for } [\text{Total X}] < 20 \mu\text{g m}^{-3}$$

$$[\text{Large X}] = [\text{Total X}], \text{ for } [\text{Total X}] \geq 20 \mu\text{g m}^{-3}$$

$$[\text{Small X}] = [\text{Total X}] - [\text{Large X}]$$

where X = sulfate, nitrate or organic mass (OM). The concentration of ammonium sulfate ($[(\text{NH}_4)_2\text{SO}_4]$) was 1.375 times the sulfate concentration ($[\text{SO}_4^{2-}]$), and the ammonium nitrate ($[\text{NH}_4\text{NO}_3]$) was 1.29 times the nitrate concentrations ($[\text{NO}_3^-]$). The OM concentration was estimated by multiplying the reported OC concentration by a factor of 1.6 (Turpin and Lim, 2001). The sea salt mass concentration was estimated by multiplying the Cl^- mass concentration by a factor of 1.8. The ammonium cation was not used directly in the IMPROVE algorithm. It was assumed to be fully neutralized by SO_4^{2-} and NO_3^- and treated as ammonium sulfate ($(\text{NH}_4)_2\text{SO}_4$) and ammonium nitrate (NH_4NO_3), respectively.

4 Results and discussion

An overview of the measurement results of the aerosol optical properties, size distribution, and chemical composition of $PM_{1.0}$ particles is shown in Table 1 and Fig. 2. There are obvious differences of the campaign average number and surface size distribution of $PM_{1.0}$ for the three

1 different pollution categories (Fig. 3). For clear days, the mean particle number size distributions
2 fitted by a mono-log normal function was around 41 nm. Bimodal distributions were observed on
3 slightly polluted and polluted days with modes centered at 38 and 105 nm (slightly polluted periods)
4 and at 38 and 151 nm (polluted periods). The mode of the number size distributions exhibits the
5 expected displacement toward the accumulation mode with increasing levels of particulate matter.

6 During the campaign, the measured aerosol extinction ($\alpha_{ep,470}$), scattering ($\alpha_{sp,470}$), and
7 absorption coefficient ($\alpha_{ap,470}$) ranged from 0.6–1165, 0.1–1150 and 0–276 Mm^{-1} , respectively. There
8 was no obvious correlation between extensive optical properties and wind direction (Fig. S4). With
9 increasing pollutant level, the extensive optical properties ($\alpha_{ep,470}$, $\alpha_{sp,470}$ and $\alpha_{ap,470}$) increased
10 strongly, in accordance with the expected, strong dependence of particle size on light scattering. In
11 contrast, changes in the intensive optical property, ω_{470} , were more modest. The optical measurement
12 data are presented as histograms of the relative frequency of occurrence of $\alpha_{ep,470}$, $\alpha_{sp,470}$, $\alpha_{ap,470}$ and
13 ω_{470} (Fig. S5) and diurnal variations of hourly averaged extinction, scattering, absorption coefficients
14 and SSA on clear, slightly polluted and polluted days are presented in Fig. S6. Diurnal variations of
15 the optical properties were broadly similar for different pollutant levels, but tended to be more
16 marked under clean conditions and modest under polluted conditions. The Huairou site is a new
17 suburban site at which aerosol optical properties have not previously been reported. To put our
18 observations at Huairou in context, the scattering and absorption coefficients and SSA observed in
19 this campaign are also compared (in the Supplement, Section S5) to those at a selection of other
20 locations (urban, suburban, and rural sites).

21 We present our results as follows: Firstly, selected periods are investigated in detail for showing
22 the process of haze formation, development and decline. The extensive optical properties (extinction,
23 scattering, and absorption coefficients) and intensive optical properties (SSA and effective CRI) are
24 presented for these periods. Secondly, the mass scattering and absorption efficiencies are determined.
25 And finally, the chemical composition on different pollution days during the campaign are
26 considered. Chemical apportionment of aerosol extinction is then studied based on the modified
27 IMPROVE algorithm.

4.1 Temporal variations of optical properties during selected air pollution episodes

The temporal variations of aerosol particle number and surface size distribution, aerosol extinction, scattering, absorption coefficients, ω_{470} , and the retrieved effective CRIs from 22 to 24 November 2014 are presented in Fig. 4. The corresponding temporal wind direction and speed are shown in the upper panel of Fig. 4, while temperature, relative humidity, pressure, and concentrations of pollutant gases (SO₂, NO₂, O₃, and CO) are shown in Fig. S7 in the Supplement. The time series of PM_{1.0} particle number distribution during the episode varied with meteorology and the sources of pollutants. To emphasize the variation of these parameters during the episode, the extended air pollution episode was divided into six shorter periods. The statistical analyses of these periods are summarized in Table 2. In the selected haze episode, these six periods show variations in the PM_{1.0} size distribution and the extensive optical properties of particles in the process of haze formation, development and decline. The evolution of intensive optical properties was related to the variation of PM_{1.0} chemical components.

24 h back trajectories starting at 200 m a.g.l. in Huairou site calculated every 4 h (at 02:00, 6:00, 10:00, 14:00, 18:00 and 22:00 LT) are shown in Fig. 5 (<http://ready.arl.noaa.gov/HYSPLIT.php>). The trajectories from the northerly direction were clean air masses with high transport heights and long transport pathways; trajectories from the southerly direction were mainly polluted air masses with low transport heights and short transport pathways.

During Period 1 and Period 6, winds were typically from the northeast; the trajectory indicated that the air masses came from cleaner air to the north and carried pollutants from northeast areas to the observation site, with concentrations of small, light absorption particles increasing. These clean air masses showed a relatively large contribution from traffic emissions. Lower values of the SSA were found during the rush hour, in common with other studies that have similarly found minimum SSA values during the morning traffic rush hour (Garland et al., 2008; Lyamani et al., 2010).

For Period 2, the air masses came from the north with clean air, but their reduced height resulted in entrainment of surface aerosols and transport to the observation site. The transport of clean, fresh air resulted in sharply decreased pollutant levels and promoted new particle formation. Takegawa et al. (2009) and Guo et al. (2014) showed that newly-formed aitken mode particles were mainly composed of sulfate and organic matter, indicating that most components were absolute scattering

1 species. In this case, the values of SSA and k should be close to 1 and 0, respectively. The retrieved
2 values of SSA (0.94 ± 0.03) and k (0.008 ± 0.005) matched these expectations and indicate that the
3 newly formed particles were predominantly scattering species.

4 For Periods 3 and 4, the shorter transport pathway of air masses suggested that the composition
5 was dominated by local emissions, including primary emissions and secondary formation. Period 3
6 was characterized by the dominance of larger accumulation mode particles for several hours. In the
7 first part of the period, the winds slowed down and turned to the south. These conditions favored
8 accumulation of local pollutants (including primary emissions and secondary production) and
9 transportation of pollutants from southern areas. Later on, the wind speed increased and the direction
10 changed to the southeast. The accumulation of pollutants brought about the formation of haze.

11 Large numbers of small, light absorbing particles were seen during Period 4, which coincided
12 with the morning rush hour. The mean values of ω_{470} and effective CRI were similar to the values in
13 Period 1 within the observed variability. During the period, weak winds from northern directions
14 transported polluted air to the observation site and resulted in higher concentrations and a greater
15 influence of light absorbing particles. The accumulation of original and newly discharged primary
16 pollutants led to sharp variations in the aerosol size distribution and extensive optical properties.
17 However, variations in the aerosol intensive optical properties were slight.

18 High extinction values were observed over Period 5, with a gradual increase and then decrease in
19 extinction, scattering, and absorption. The mean values of ω_{470} , n and k were 0.86 ± 0.01 , 1.44 ± 0.03 ,
20 and 0.02 ± 0.01 , respectively. The SSA values were larger than those reported for Period 4. In
21 general, the n values were higher and the k values lower than those seen in Period 4, although the
22 mean values of both properties fall within the combined standard deviations of both periods. For this
23 period, the airflow passed over the Beijing city area and over the southwestern direction of the
24 observation site, bringing surface air pollutants to the Huairou site and contributing to the formation
25 of serious haze. Both the mean diameter of the number and surface size distribution (124 ± 19 and
26 263 ± 11 nm) and n were larger in this period than in the other five periods. The light scattering
27 efficiency increased with the increment of the particle size.

28 According to the regulatory classification of the atmospheric pollution level, these six periods
29 can be divided into two categories: clear day (22:00 LT 21 November–10:00 LT 22 November) and
30 polluted day (10:00 LT 22 November–22:00 LT 22 November, 22:00 LT 22 November–10:00 LT 23

1 November, 10:00 LT 23 November–22:00 LT 23 November, 22:00 LT 23 November–10:00 LT 24
2 November). The mean value of the total mass concentration on clear days was $9.49 \mu\text{g m}^{-3}$, and the
3 mean fractional contributions of OM, nitrate, and sulfate were 56% ($5.32 \mu\text{g m}^{-3}$), 12% ($1.12 \mu\text{g m}^{-3}$),
4 and 14% ($1.34 \mu\text{g m}^{-3}$), respectively. On polluted days, the mean value of the total mass
5 concentration was $41.6 \mu\text{g m}^{-3}$ with fractional contributions of 44% OM ($18.5 \mu\text{g m}^{-3}$), 22% nitrate
6 ($9.3 \mu\text{g m}^{-3}$), and 11% sulfate ($4.5 \mu\text{g m}^{-3}$). In summary, in going from clear to polluted days, the
7 fractional contribution of OM to the total mass decreased by 12%, whereas the fraction of nitrate
8 almost doubled and that of sulfate decreased slightly. Organic matter was the largest contributor to
9 $\text{PM}_{1.0}$. The notable increase in the concentration and fractional contribution to $\text{PM}_{1.0}$ extinction
10 coefficient of inorganic species, and specifically nitrate and ammonium, indicate that the inorganic
11 contribution to particulate matter becomes relatively more important than the OM fraction during
12 haze. The chemical composition is discussed further in Section 4.3.

14 4.2 Mass scattering and mass absorption efficiencies

16 MSE and MAE of $\text{PM}_{1.0}$

18 Figure 6 shows the relationship between the scattering and absorption coefficients and $\text{PM}_{1.0}$
19 mass concentrations under different pollution levels. The $\text{PM}_{1.0}$ mass concentrations were determined
20 by multiplying the volume concentrations with the volume-weighted mass density of each filter
21 sample (Hasan and Dzubay, 1983). The scattering and (to a lesser extent) the absorption coefficients
22 were generally well correlated with the $\text{PM}_{1.0}$ mass concentrations and have small y-intercepts. (The
23 larger deviation of the y-intercept on polluted days likely stems from the smaller number of low mass
24 concentration observations on these days.)

25 The derived $\text{PM}_{1.0}$ average mass scattering and absorption efficiencies during the campaign were
26 3.60 and $0.70 \text{ m}^2 \text{ g}^{-1}$, respectively (Fig. 6d). Statistical uncertainties from the slope of the regression
27 are misleadingly small and have been omitted in the reported MSE and MAE values. The MSE and
28 MAE values are smaller than those observed by Garland et al. (2008) from suburban Guangzhou in
29 July 2006 (where the $\text{PM}_{1.0}$ mass scattering and absorption efficiency calculated assuming an average
30 effective density of ammonium sulfate (1.7 g cm^{-3}) were 4.13 and $1.09 \text{ m}^2 \text{ g}^{-1}$, respectively), the

1 value of $PM_{2.5}$ at $\lambda = 520$ nm obtained in urban Beijing ($4.8 \text{ m}^2 \text{ g}^{-1}$) during wintertime (Tao et al.,
2 2015), and in Chengdu and Guangzhou ($3.9 \text{ m}^2 \text{ g}^{-1}$) (Tao et al., 2014a, b). The derived mass
3 extinction efficiency is $4.30 \text{ m}^2 \text{ g}^{-1}$, which was comparable to the reported values during Aerosols
4 1999 ($4.1\text{--}5.4 \text{ m}^2 \text{ g}^{-1}$) (Quinn et al., 2001) and INDOEX 1999 ($4.0\text{--}5.6 \text{ m}^2 \text{ g}^{-1}$) (Quinn et al., 2002).

5 In this work, the MSE of $PM_{1.0}$ was $4.16 \text{ m}^2 \text{ g}^{-1}$ during polluted days, which was 34% higher
6 than that during the slightly polluted days ($3.11 \text{ m}^2 \text{ g}^{-1}$) and 75% higher than that during the clear
7 days ($2.38 \text{ m}^2 \text{ g}^{-1}$) (Fig. 6a–c). The variability in MSE typically depends more on the mass size
8 distribution than on density or refractive index (Hand and Malm, 2007). As shown in Fig. 3, the
9 particle diameter increased significantly with high aerosol mass concentrations. The MSEs in this
10 work increased consistently with pollution level, primarily because larger particles scatter light more
11 efficiently. Cheng et al. (2015) showed that the MSEs of ammonium nitrate, ammonium sulfate and
12 organic matter increased rapidly with increasing mass concentration at lower aerosol loadings, while
13 the MSEs of ammonium nitrate and ammonium sulfate fluctuated in a narrow range under high
14 aerosol loading conditions when the MSE of organic matter was slightly smaller. One recent study
15 (Tao et al., 2015) showed that the MSE was determined by the proportions of the dominant chemical
16 components and their size distributions under different pollution levels. The MSEs in this work
17 increased consistently with the mass concentration of particles because of the relationship between
18 size and light scattering efficiency.

19

20 MAE of EC

21

22 Similar time profiles are seen for the measured absorption coefficient at $\lambda = 470$ nm and the
23 measured mass concentrations of EC and OC (Fig. 7 (a) and (b)). Assuming that only EC contributes
24 to aerosol absorption, the MAE of EC can be calculated using Eq. (4). The MAE values of EC at $\lambda =$
25 470 nm over the campaign period are shown in Fig. 7 (c). These values vary widely, with lower
26 values generally seen under cleaner conditions and higher values observed under more polluted
27 conditions. The MAE values for selected clear days (e.g. Nov. 17 - 18; Dec. 1 - Dec. 3; Dec. 29, 2014
28 - Jan. 1, 2015) ranged from $7 - 14 \text{ m}^2 \text{ g}^{-1}$ (average of $10.3 \pm 2.7 \text{ m}^2 \text{ g}^{-1}$) and are comparable to those
29 reported in Beijing during the summer ($5 - 13 \text{ m}^2 \text{ g}^{-1}$) (Cheng et al., 2011). Much higher values were
30 seen on polluted days, where the MAE ranged from 23 to $81 \text{ m}^2 \text{ g}^{-1}$ (average of $48 \pm 21 \text{ m}^2 \text{ g}^{-1}$) for

1 the period covered Dec. 23 - 28, 2014 and from 20 to 49 $\text{m}^2 \text{g}^{-1}$ (average of $42 \pm 14 \text{m}^2 \text{g}^{-1}$) for Jan. 2
2 - 5, 2015. These values are comparable to those reported by Chan et al. (2011), where MAE ranged
3 from 10 to $50 \text{m}^2 \text{g}^{-1}$.

4 The average EC mass concentrations were $0.48 \pm 0.39 \mu\text{g m}^{-3}$, $1.18 \pm 0.59 \mu\text{g m}^{-3}$, and $2.72 \pm$
5 $0.87 \mu\text{g m}^{-3}$, for clear, slightly polluted, and polluted days, respectively. The corresponding mass
6 fractions of $4.3 \pm 3.6\%$, $4.0 \pm 2.0\%$, and $3.6 \pm 1.1\%$ were approximately equal within the large
7 variability seen on different days. The mean and standard deviations of MAE values of EC were 23.0
8 $\pm 14.0 \text{m}^2 \text{g}^{-1}$, $32.7 \pm 16.0 \text{m}^2 \text{g}^{-1}$, and $35.0 \pm 21.7 \text{m}^2 \text{g}^{-1}$, respectively, for clear, slightly polluted, and
9 polluted days. Our values suggest that EC absorption was strongly enhanced over the campaign
10 period. Enhanced absorption (E_{abs}) could arise from the coating-enhancement of ambient BC
11 absorption (lensing-driven enhancement), as well as absorption associated with light-absorbing
12 organic compounds (brown carbon, BrC) (Andreae and Gelencsér 2006; Bond et al., 2013;
13 Gustafsson, and Ramanathan, 2016). In general, light absorption from other organic species tends to
14 be relatively small at $\lambda = 470 \text{nm}$, whether it arises from small nitroaromatic compounds (Claeys et
15 al., 2012) or from larger HULIS-type substances (Lorenzo and Young, 2016).

16 Laboratory studies report a BC enhancement factor from 1.8 to 2 for thicker coatings (Bond et
17 al., 2013). Results from field observations are more variable (Peng et al., 2016): reported E_{abs} values
18 ranged from 1.06 (Cappa et al. 2012; Lan et al., 2013) to 1.7 (Lack et al. 2012; Liu et al., 2015),
19 although two recent studies (Cui et al., 2016; Peng et al., 2016) have found that for aged BC (18 h
20 and 4.6 h after fresh emission in clear and polluted condition, respectively), E_{abs} ranged from 2 to 3.
21 Compared to freshly emitted BC, we observe average absorption enhancements of 2.6 (clear), 3.8
22 (slightly polluted), and 4.0 (polluted) for different days. Our values are somewhat higher, although
23 broadly consistent with, the Peng (2016).

24 Our individual MAE of EC values are often appreciably higher than has been observed in other
25 studies (Andreae et al., 2008; Cheng et al., 2011; Wang et al., 2014). This difference may arise from
26 either measurement uncertainties or the contribution of other absorbing species. Large MAE values
27 could arise in part from inaccuracies in both the EC mass concentration or α_{abs} (which is itself
28 determined from the relatively small difference between the extinction and scattering measurements).
29 Moreover, our assumption that all particle absorption arises from EC would lead to higher MAE
30 values if there was simultaneous absorption by other species. L. Wang et al. (2013) have recently

1 shown that BrC was the second-largest absorbing aerosol constituent in Beijing (with a volume
2 fraction of 5 - 25% in the total aerosol volume) and exhibits a clear seasonal variation (dominates in
3 late fall and winter, and extremely low in summer). The sources of BrC have been reported to be the
4 organic components primary emitted from the combustion of biomass and fossil fuels. In a study of
5 biomass burning particle, Lack et al. (2012) showed that the contribution of the absorption of BrC
6 was about 27% at $\lambda = 404$ nm, while other recent studies (Nakayama et al., 2013; Moise et al., 2015)
7 have shown that secondary organic aerosol may also act as BrC.

8 Our data provide some support for the suggestion that SOA is absorbing. Since primary OC and
9 EC are mostly emitted from the same source, EC is a good tracer of primary combustion-generated
10 carbon emissions and the OC/EC ratio can be used as an indicator for the formation of SOA (Cheng
11 et al., 2011). Time-resolved OC and EC data provide a better understanding of the dynamics of SOA
12 formation. In this work, the pattern of MAE coincided well with OC/EC ratio, suggesting that SOA
13 has a non-negligible absorption on polluted days. This also implies that our MAE values reported
14 above are upper limits, and that the absorption contribution of EC is likely to be somewhat smaller.

16 4.3 Chemical composition and light extinction apportionment on different air pollution days

18 Chemical composition

20 Table 1 and Fig. 8 show the mean mass concentration values and the mean percentile
21 compositions of observed chemical compositions of PM_{1.0} particles under different pollution levels.
22 The contribution of sulfate, nitrate and ammonium to the observed PM_{1.0} mass concentration
23 increased strongly on polluted compared to clear days (from 34 to 44%). Similar trends were
24 observed for PM_{2.5} and NR-PM_{1.0} during the January 2013 severe haze events in Beijing (Sun et al.,
25 2014; Tao et al., 2015; G. J. Zheng et al., 2015).

26 On average, OM, nitrate, sulfate, ammonium, chloride and EC comprised 46.3% ($13.3 \pm 11.1 \mu\text{g}$
27 m^{-3}), 18.0% ($5.2 \pm 5.5 \mu\text{g} \text{m}^{-3}$), 11.6% ($3.3 \pm 3.5 \mu\text{g} \text{m}^{-3}$), 10.3% ($3.0 \pm 3.6 \mu\text{g} \text{m}^{-3}$), 5.3% (1.5 ± 1.9
28 $\mu\text{g} \text{m}^{-3}$) and 3.9% ($1.1 \pm 0.9 \mu\text{g} \text{m}^{-3}$) of observed PM_{1.0}, respectively. The organic mass was the
29 largest proportion in PM_{1.0} particles, and the contribution of nitrate was larger than that of sulfate.
30 Compared to summer, the mass contribution of organics was significantly higher during winter, and

1 primary organic aerosol dominated during the coal heating season (Sun et al., 2013). Huang et al.
2 (2014) reported that secondary organic aerosol (SOA) contributed 26% of PM_{2.5} in Beijing in the
3 January 2013 severe haze events, and indicated the dominant effect of fossil fuel SOA formation in
4 Beijing regions.

5 Compared to sulfate, the fractional composition of nitrate and ammonium aerosol increased
6 under high levels of pollution. Similar increases in the proportion of secondary inorganic species,
7 and particularly nitrates, have been observed during other haze episodes in the North China Plain and
8 other Chinese megacities (Pathak et al., 2009; Jansen et al., 2014; Tian et al., 2015). Based on the
9 relative abundances of nitrate and ammonium, these increases have been attributed to gas phase
10 formation of nitrate from HNO₃ and NH₃. In our results, the molar ratios [NO₃]/[SO₄] and
11 [NH₄]/[SO₄] fall between 2.1 to 2.5, and 3.0 to 5.2, respectively (based on the mean concentrations
12 of these components), and are consistent with this explanation for an ammonium-rich regime (Pathak
13 et al., 2009; Tian et al., 2015). It is worth noting that the increases in secondary inorganic species is
14 not universal: some studies have reported haze episodes (or portions of such episodes) in which the
15 organic fraction increases substantially (Tian et al., 2015; Wang et al., 2015). This difference likely
16 reflects the relative importance of sources and atmospheric processing in both the gas and liquid
17 phases during such events (Tian et al., 2016).

18

19 **Chemical apportionment of aerosol optical properties**

20

21 Over the past years, the chemical apportionment of α_{ep} or α_{sp} has been conducted in both urban
22 and non-urban regions (Malm et al., 1994; Watson, 2002; Cheung et al., 2005; Malm and Hand, 2007;
23 Yang et al., 2007; Tao et al., 2009; Cao et al., 2012; Han et al., 2014; Tao et al., 2014a; Cheng et al.,
24 2015). Ammonium sulfate was generally the largest contributor to PM_{2.5} or PM₁₀ α_{ep} , with a range
25 from 20–50%. However, fewer studies have been reported of the chemical contribution of different
26 chemical components to the extinction of PM_{1.0} under different pollution levels.

27 In this work, the average fractional contributions of each chemical component of dry PM_{1.0}
28 extinction coefficient with respect to different pollution levels were calculated with the IMPROVE
29 algorithm (Fig. 9). The optical extinction of OM, ammonium nitrate, ammonium sulfate, elemental
30 carbon and sea salt accounted for 57.9, 17.8, 12.5, 8.6 and 3.2 % of the reconstructed PM_{1.0}

1 extinction in this campaign, respectively. The contribution of chemical compositions to aerosol
2 extinction depends mainly on their mass concentrations. OM, ammonium nitrate, ammonium sulfate,
3 element carbon and sea salt accounted for 50.4, 21.2, 16.8, 4.2 and 7.4 % of the reconstructed PM_{1.0}
4 mass concentrations, respectively. The organic constituents comprised a large fraction of PM_{1.0} mass
5 concentration, consistent with previous studies (Yao et al., 2010; Sun et al., 2013), and therefore
6 made the largest contribution to the extinction of PM_{1.0} particles in this study. The relative
7 contribution of OM (58 %) to the total extinction reported here was comparable to that previously
8 reported in Beijing (54 %) during an extreme haze episode in January 2013 for PM_{1.0} scattering
9 (Wang et al., 2015), and in Shenzhen (45 %) in the winter of 2009 for PM_{2.5} extinction (Yao et al.,
10 2010). The contribution of organics in Beijing increases during the winter coal heating season (Sun
11 et al., 2013). Emissions from the large number of vehicles in the mega-cities of China also contribute
12 significantly to organic aerosol (Huang et al., 2014). From clear days to slightly polluted days, the
13 relative contribution of organic mass to light extinction increased by 7 %, which may due to an
14 increasing contribution of secondary organic aerosol (SOA) (Huang et al., 2014). The concentrations
15 of nitrate and ammonium aerosol increased under high levels of pollution, and the relative
16 contribution of ammonium nitrate to PM_{1.0} light extinction increased by 6.7 % under these conditions
17 (Wang et al., 2015).

18 The parameterization of EC extinction in the modified IMPROVE algorithm is based on the
19 optical properties of freshly emitted EC. However, Section 4.2 showed that, both in our work and in
20 previous studies, EC absorption in ambient aerosols is enhanced several-fold. Not accounting for the
21 effective absorption of EC will underestimate the extinction, as in indeed borne out in the correlation
22 between calculated and measured extinctions (Fig. S3(c)). To address this issue, we investigated
23 parameterizing the IMPROVE algorithm based on the absorption enhancement of 2.4-fold recently
24 reported by Peng et al. (2016). The BC term in the modified IMPROVE function was changed as
25 follows: (1) an absorption enhancement factor of 2.4 gave a new MAE value of 20.9 m² g⁻¹ for BC at
26 $\lambda = 470$ nm; and (2) a scattering contribution from EC (based on an SSA of 0.2 (Bond and Bergstrom,
27 2006)), produced a MSE value of 2.18 m² g⁻¹ for BC. The MEE term (10.8 m² g⁻¹) in the modified
28 IMPROVE was replaced with the summation of the two parts (23 m² g⁻¹ at $\lambda = 470$ nm). These
29 changes raised the calculated aerosol extinction by 8% (Fig. S10), thereby improving the agreement
30 with measurements. The deviation of the correlation between calculations and measurements from

1 unity was reduced from 23% to 15%. The revised MEE of EC doubled the contribution of EC to the
2 total aerosol extinction from 8.7% to 17% (Fig. S11). The SSA from the IMPROVE calculations
3 accordingly decreased from 0.91 to 0.83, in much better agreement with the mean measured SSA of
4 0.80. We therefore recommend implementing these changes to the MEE of EC when applying the
5 IMPROVE algorithm, particularly in polluted environments.

6 The contribution of EC to the total extinction is therefore considerable, despite contributing only
7 4% to the total aerosol mass. Major sources of EC in the NCP include coal consumption, biomass
8 burning and vehicle exhaust. In the context of several haze episodes in the NCP, recent modeling
9 studies have shown that EC, as the major absorbing component of aerosols, causes local atmospheric
10 heating and thereby exacerbates aerosol pollution by reducing the planetary boundary layer height
11 (Ding et al., 2016; Gao et al., 2015; Gao et al., 2016). The disproportionately large effect of EC
12 observed in our study supports the suggestion in these papers that targeting the reduction of EC
13 emissions will pay off both in improving air quality and reducing climate impacts.

14

15 **5 Summary and conclusions**

16

17 $PM_{1.0}$ optical properties and composition at a suburban site near Beijing were measured during
18 the HOPE-J³A campaign. Six periods were investigated in detail to study the evolution of intensive
19 optical properties and chemical composition in $PM_{1.0}$ during an extended haze episode. Our analysis
20 reveals that the optical properties of aerosols change significantly during the evolution of haze.

21 The mass concentrations of sulfate, nitrate, and ammonium species were high during haze
22 episodes. Organic matter was consistently the dominant constituent by mass of the observed aerosols,
23 and light extinction apportionment indicated that was it accordingly made the largest contribution to
24 the extinction of $PM_{1.0}$. Under polluted conditions, the proportion of inorganic components,
25 especially nitrate, was higher than under clean conditions and the contribution of inorganic
26 components to visibility degradation was significant.

27 Under polluted conditions, the average MAE of EC were up to 4 times as large as the reference
28 MAE value for freshly emitted BC. The temporal pattern of MAE values was similar to that of the
29 OC/EC ratio, suggesting that some non-BC absorption from SOA also contributes to particle
30 absorption. After considering the coating enhanced absorption by EC, agreement with measurements

1 was improved with the new modified IMPROVE algorithm. Organic mass was the largest
2 contributor (52%) to the total extinction of PM_{1.0}, while EC, despite its mass concentration being
3 only 4%, contributed about 17%, to extinction. EC, owing to its high absorption efficiency,
4 contributed appreciably to PM_{1.0} extinction and should be a key target to air quality controls.

5
6 *Acknowledgements.* The authors wish thank to Zhouqing Xie at University of Science and
7 Technology of China for providing the meteorological data used in this paper and to Jun Tao and
8 Zejian Lin at South China Institute of Environmental Science for helpful discussion. This research
9 was supported by the National Natural Science Foundation of China (41330424), the Natural Science
10 Foundation of Anhui Province (1508085J03), the Key Research Program of the Chinese Academy of
11 Sciences (KJZD-EW-TZ-G06-01), and the China Special Fund for Meteorological Research in the
12 Public Interest (GYHY201406039). The support of the CaPPA project (“Chemical and Physical
13 Properties of the Atmosphere”), funded by the French National Research Agency through the
14 “Programme d’Investissement d’Avenir” (under contract ANR-10-LABX-005), is acknowledged.
15 We thank the reviewers and editor for their constructive suggestions.

17 **References**

- 18
19 Abo Riziq, A., Erlick, C., Dinar, E., and Rudich, Y.: Optical properties of absorbing and
20 non-absorbing aerosols retrieved by cavity ring down (CRD) spectroscopy, *Atmos. Chem.*
21 *Phys.*, 7, 1523–1536, doi:10.5194/acp-7-1523-2007, 2007.
- 22 Anderson, T. L., Charlson, R. J., Schwartz, S. E., Knutti, R., Boucher, O., Rodhe, H., and
23 Heintzenberg, J.: Atmospheric science. Climate forcing by aerosol – a hazy picture, *Science*,
24 300, 1103–1104, 2003.
- 25 Andersson, A., Deng, J., Du, K., Zheng, M., Yan, C., Skold, M., and Gustafsson, O.:
26 Regionally varying combustion sources of the January 2013 severe haze events over eastern
27 China, *Environ. Sci. Technol.*, 49, 2038–2043, doi:10.1021/es503855e, 2015.
- 28 Andreae, M. O. and Gelencsér, A.: Black carbon or brown carbon? The nature of light-absorbing
29 carbonaceous aerosols, *Atmos. Chem. Phys.*, 6, 3131–3148, doi:10.5194/acp-6-3131-2006,
30 2006.
- 31 Andreae, M.O., Schmid, O., Yang, H., Chand, D., Yu, J.Z., Zeng, L.-M., and Zhang, Y.-H.: Optical
32 properties and chemical composition of the atmospheric aerosol in urban Guangzhou, China,
33 *Atmos. Environ.*, 42, 6335–6350, 2008.
- 34 Bahadur, R., Praveen, P. S., Xu, Y., and Ramanathan, V.: Solar absorption by elemental and brown
35 carbon determined from spectral observations, *P. Natl. Acad. Sci. USA*, 109, 17366–17371,
36 2012.

- 1 Bates, T. S., Huebert, B. J., Gras, J. L., Griffiths, F. B., and Durkee, P. A.: International Global
2 Atmospheric Chemistry (IGAC) project's first aerosol characterization experiment (ACE 1):
3 overview, *J. Geophys. Res.*, 103, 16297–16318, doi:10.1029/97jd03741, 1998.
- 4 Bates, T. S., Anderson, T. L., Baynard, T., Bond, T., Boucher, O., Carmichael, G., Clarke, A., Erlick,
5 C., Guo, H., Horowitz, L., Howell, S., Kulkarni, S., Maring, H., McComiskey, A.,
6 Middlebrook, A., Noone, K., O'Dowd, C. D., Ogren, J., Penner, J., Quinn, P. K., Ravishankara,
7 A. R., Savoie, D. L., Schwartz, S. E., Shinozuka, Y., Tang, Y., Weber, R. J., and Wu, Y.:
8 Aerosol direct radiative effects over the northwest Atlantic, northwest Pacific, and North
9 Indian Oceans: estimates based on in-situ chemical and optical measurements and chemical
10 transport modeling, *Atmos. Chem. Phys.*, 6, 1657–1732, doi:10.5194/acp-6-1657-2006, 2006.
- 11 Bond, T. C., Doherty, S. J., Fahey, D. W., Forster, P. M., Berntsen, T., DeAngelo, B. J., Flanner, M.
12 G., Ghan, S., Kärcher, B., Koch, D., Kinne, S., Kondo, Y., Quinn, P. K., Sarofim, M. C.,
13 Schultz, M. G., Schulz, M., Venkataraman, C., Zhang, H., Zhang, S., Bellouin, N., Guttikunda,
14 S. K., Hopke, P. K., Jacobson, M. Z., Kaiser, J. W., Klimont, Z., Lohmann, U., Schwarz, J. P.,
15 Shindell, D., Storelvmo, T., Warren, S. G., and Zender C. S.: Bounding the role of black carbon
16 in the climate system: A scientific assessment, *J. Geophys. Res. Atmos.*, 118, 5380 - 5552,
17 doi:10.1002/jgrd.50171, 2013.
- 18 Bond, T. C., Habib, G., and Bergstrom, R. W.: Limitations in the enhancement of visible light
19 absorption due to mixing state, *J. Geophys. Res.*, 111(D20), 211, doi:10.1029/2006JD007315,
20 2006.
- 21 Cahill, J. F., Suski, K., Seinfeld, J. H., Zaveri, R. A., and Prather, K. A.: The mixing state of
22 carbonaceous aerosol particles in northern and southern California measured during CARES
23 and CalNex 2010, *Atmos. Chem. Phys.*, 12, 10989–11002, doi:10.5194/acp-12-10989-2012,
24 2012.
- 25 Cao, J., Chow, J. C., Lee, F. S. C., and Watson, J. G.: Evolution of PM_{2.5} measurements and
26 standards in the US and future perspectives for china, *Aerosol Air Qual. Res.*, 13, 1197–1211,
27 2013.
- 28 Cao, J. J., Wang, Q. Y., Chow, J. C., Watson, J. G., Tie, X. X., Shen, Z. X., Wang, P., and An, Z. S.:
29 Impacts of aerosol compositions on visibility impairment in Xi'an, China, *Atmos. Environ.*, 59,
30 559–566, doi:10.1016/j.atmosenv.2012.05.036, 2012.
- 31 Cappa, C. D., Onasch, T. B., Massoli, P., Worsnop, D. R., Bates, T. S., Cross, E. S., Davidovits, P.,
32 Hakala, J., Hayden, K. L., Jobson, B. T., Kolesar, K. R., Lack, D. A., Lerner, B. M., S. M.,
33 Mellon, D., Nuaaman, I., Olfert, J. S., Petäjä, T., Quinn, P. K., Song, C., Subramanian, R.,
34 Williams, E. J., and Zaveri, R. A. : Radiative absorption enhancements due to the mixing state
35 of atmospheric black carbon, *Science*, 337, 1078 - 1081, doi:10.1126/science.1223447, 2012.
- 36 Chan, T. W., Brook, J. R., Smallwood, G. J., and Lu, G.: Time resolved measurements of black
37 carbon light absorption enhancement in urban and near-urban locations of southern Ontario,
38 Canada, *Atmos. Chem. Phys.*, 11, 10407 - 10432, doi:10.5194/acp-11-10407-2011, 2011.
- 39 Cheng, Y., He, K.-B., Zheng, M., Duan, F.-K., Du, Z.-Y., Ma, Y.-L., Tan, J.-H., Yang, F.-M., Liu,
40 J.-M., Zhang, X.-L., Weber, R. J., Bergin, M. H., and Russell, A. G.: Mass absorption
41 efficiency of elemental carbon and water-soluble organic carbon in Beijing, China, *Atmos.*
42 *Chem. Phys.*, 11, 11497-11510, doi:10.5194/acp-11-11497-2011, 2011.
- 43 Cheng, Y., Engling, G., Moosmüller, H., Arnott, W.P., Chen, L.W.A., Wolde, C. E., Min Hao, W.M.,
44 and He, K.B.: Light absorption by biomass burning source emissions, *Atmos. Environ.*, 127,

1 347 - 354, 2016.

2 Cheng, Y. F., Wiedensohler, A., Eichler, H., Su, H., Gnauk, T., Brüggemann, E., Herrmann, H.,
3 Heintzenberg, J., Slanina, J., Tuch, T., Hu, M., and Zhang, Y. H.: Aerosol optical properties
4 and related chemical apportionment at Xinken in Pearl River Delta of China, *Atmos. Environ.*,
5 30 42, 6351–6372, doi:10.1016/j.atmosenv.2008.02.034, 2008.

6 Cheng, Z., Jiang, J., Chen, C., Gao, J., Wang, S., Watson, J. G., Wang, H., Deng, J., Wang, B., Zhou,
7 M., Chow, J. C., Pitchford, M. L., and Hao, J.: Estimation of aerosol mass scattering
8 efficiencies under high mass loading: case study for the megacity of Shanghai, China, *Environ.*
9 *Sci. Technol.*, 49, 831–838, doi:10.1021/es504567q, 2015.

10 Cheung, H. C., Wang, T., Baumann, K., and Guo, H.: Influence of regional pollution outflow on the
11 concentrations of fine particulate matter and visibility in the coastal area of southern China,
12 *Atmos. Environ.*, 39, 6463–6474, doi:10.1016/j.atmosenv.2005.07.033, 2005.

13 Chu, D. A., Kaufman, Y. J., Zibordi, G., Chern, J. D., Mao, J. T., Li, C. C., and Holben, B. N.:
14 Global monitoring of air pollution over land from the Earth Observing System-Terra Moderate
15 Resolution Imaging Spectroradiometer (MODIS), *J. Geophys. Res.*, 108(D21), 4661, 2003.

16 Claeys, M., Vermeylen, R., Yasmeen, F., Gómez-González, Y., Chi, C., Maenhaut, W., Mészáros, T.,
17 and Salma, I.: Chemical characterisation of humic-like substances from urban, rural and
18 tropical biomass burning environments using liquid chromatography with UV/vis photodiode
19 array detection and electrospray ionisation mass spectrometry, *Environ. Chem.*, 9, 273-284,
20 2012.

21 Cui, X., Wang, X., Yang, L., Chen, B., Chen, J., Andersson, A., and Gustafsson, Ö. : Radiative
22 absorption enhancement from coatings on black carbon aerosols, *Sci. Total Environ.* 551-552,
23 51 - 56, 2016.

24 Di Lorenzo, R. A., and Young C. J.: Size separation method for absorption characterization in brown
25 carbon: Application to an aged biomass burning sample, *Geophys. Res. Lett.*, 43, 458–465,
26 doi:10.1002/2015GL066954, 2016.

27 Dinar, E., Abo Riziq, A., Spindler, C., Erlick, C., Kiss, G., and Rudich, Y.: The complex refractive
28 index of atmospheric and model humic-like substances (HULIS) retrieved by a cavity ring
29 down aerosol spectrometer (CRD-AS), *Faraday Discuss.*, 137, 279–295, 2008.

30 Ding, A. J., Huang, X., Nie, W., Sun, J. N., Kerminen, V.-M., Petäjä, T., Su, H., Cheng, Y. F., Yang,
31 X.-Q., Wang, M. H., Chi, X. G., Wang, J. P., Virkkula, A., Guo, W. D., Yuan, J., Wang, S. Y.,
32 Zhang, R. J., Wu, Y. F., Song, Y., Zhu, T., Zilitinkevich, S., Kulmala, M., and Fu, C. B.:
33 Enhanced haze pollution by black carbon in megacities in China, *Geophys. Res. Lett.*, 43, 2873
34 - 2879, doi:10.1002/2016GL067745, 2016.

35 Doherty, S. J., Quinn, P. K., Jefferson, A., Carrico, C. M., Anderson, T. L., and Hegg, D.: A
36 comparison and summary of aerosol optical properties as observed in situ from aircraft, ship,
37 and land during ACE-Asia, *J. Geophys. Res.*, 110, D04201, doi:10.1029/2004jd004964, 2005.

38 Eldering, A., Ogren, J. A., Chowdhury, Z., Hughes, L. S., and Cass, G. R.: Aerosol optical properties
39 during INDOEX based on measured aerosol particle size and composition, *J. Geophys. Res.*,
40 107, 8001, doi:10.1029/2001jd001572, 2002.

41 Fiedler, S. E., Hese, A., and Ruth, A. A.: Incoherent broad-band cavity-enhanced absorption
42 spectroscopy, *Chem. Phys. Lett.*, 371, 284–294, 2003.

43 Gao, Y., Zhang, M., Liu, Z., Wang, L., Wang, P., Xia, X., Tao, M., and Zhu, L.: Modeling the
44 feedback between aerosol and meteorological variables in the atmospheric boundary layer

1 during a severe fog–haze event over the North China Plain, *Atmos. Chem. Phys.*, 15,
2 4279–4295, doi:10.5194/acp-15-4279-2015, 2015.

3 Gao, M., Carmichael, G. R., Wang, Y., Saide, P. E., Yu, M., Xin, J., Liu, Z., and Wang, Z.:
4 Modeling study of the 2010 regional haze event in the North China Plain, *Atmos. Chem. Phys.*,
5 16, 1673–1691, doi:10.5194/acp-16-1673-2016, 2016.

6 Garland, R. M., Yang, H., Schmid, O., Rose, D., Nowak, A., Achtert, P., Wiedensohler, A.,
7 Takegawa, N., Kita, K., Miyazaki, Y., Kondo, Y., Hu, M., Shao, M., Zeng, L. M., Zhang, Y. H.,
8 Andreae, M. O., and Pöschl, U.: Aerosol optical properties in a rural environment near the
9 mega-city Guangzhou, China: implications for regional air pollution, radiative forcing and
10 remote sensing, *Atmos. Chem. Phys.*, 8, 5161–5186, doi:10.5194/acp-8-5161-2008, 2008.

11 Garland, R. M., Schmid, O., Nowak, A., Achtert, P., Wiedensohler, A., Gunthe, S. S., Takegawa, N.,
12 Kita, K., Kondo, Y., Hu, M., Shao, M., Zeng, L. M., Zhu, T., Andreae, M. O., and Pöschl, U.:
13 Aerosol optical properties observed during Campaign of Air Quality Research in Beijing 2006
14 (CAREBeijing-2006): characteristic differences between the inflow and outflow of Beijing city
15 air, *J. Geophys. Res.*, 114, D00g04, doi:10.1029/2008jd010780, 2009.

16 Gustafssona, Ö., and Ramanathan, V.: Convergence on climate warming by black carbon aerosols,
17 *Proc. Nat. Acad. Sci. USA*, 113, 4243–4245, doi: 10.1073/pnas.1603570113, 2016.

18 Guo, S., Hu, M., Zamora, M. L., Peng, J., Shang, D., Zheng, J., Du, Z., Wu, Z., Shao, M., Zeng, L.,
19 Molina, M. J., and Zhang, R.: Elucidating severe urban haze formation in China, *P. Natl. Acad.*
20 *Sci. USA*, 111, 17373–17378, 2014.

21 Han, B., Zhang, R., Yang, W., Bai, Z., Ma, Z., and Zhang, W.: Heavy air pollution episodes in
22 Beijing during January 2013: inorganic ion chemistry and source analysis using Highly Time-
23 Resolved Measurements in an urban site, *Atmos. Chem. Phys. Discuss.*, 15, 11111–11141,
24 doi:10.5194/acpd-15-11111-2015, 2015.

25 Han, L., Zhou, W., and Li, W.: Increasing impact of urban fine particles (PM_{2.5}) on areas
26 surrounding Chinese cities, *Scientific Reports*, 5, 12467, doi:10.1038/srep12467, 2015.

27 Han, T. T., Liu, X. G., Zhang, Y. H., Qu, Y., Gu, J. W., Ma, Q., Lu, K. D., Tian, H. Z., Chen, J.,
28 Zeng, L. M., Hu, M., and Zhu, T.: Characteristics of aerosol optical properties and their
29 chemical apportionments during CAREBeijing 2006, *Aerosol Air Qual. Res.*, 14, 1431–1442,
30 2014.

31 Hand, J. L., and Malm, W. C.: Review of aerosol mass scattering efficiencies from ground-based
32 measurements since 1990, *J. Geophys. Res.*, 112, D16203, doi:10.1029/2007JD008484, 2007.

33 Hasan, H. and Dzubay, T. G.: Apportioning light extinction coefficients to chemical species in
34 atmospheric aerosol, *Atmos. Environ.*, 17, 1573–1581, 1983.

35 Huang, R. J., Zhang, Y., Bozzetti, C., Ho, K.-F., Cao, J., Han, Y., Dällenbach, K. R., Slowik, J. G.,
36 Platt, S. M., Canonaco, F., Zotter, P., Wolf, R., Pieber, S. M., Bruns, E. A., Crippa, M., Ciarelli,
37 G., Piazzalunga, A., Schwikowski, M., Abbazade, G., Schnelle-Kreis, J., Zimmermann, R.,
38 An, Z., Szidat, S., Baltensperger, U., Haddad, I. E., and Prévôt, A. S. H.: High secondary
39 aerosol contribution to particulate pollution during haze events in China, *Nature*, 514, 218–222,
40 2014.

41 Jansen, R.C., Shi, Y., Chen, J., Hu, Y., Xu, C., Hong, S., Li, J., and Zhang, M.: Using hourly
42 measurements to explore the role of secondary inorganic aerosol in PM_{2.5} during haze and fog
43 in Hangzhou, China, *Adv. Atmos. Sci.*, 31, 1427 - 1434, 2014.

44 Jung, J., Lee, H., Kim, Y. J., Liu, X. G., Zhang, Y. H., Hu, M., and Sugimoto, N.: Optical properties

- 1 of atmospheric aerosols obtained by in situ and remote measurements during 2006 Campaign
2 of Air Quality Research in Beijing (CAREBeijing-2006), *J. Geophys. Res.*, 114, D00g02,
3 doi:10.1029/2008jd010337, 2009.
- 4 Knox, A., Evans, G. J., Brook, J. R., Yao, X., Jeong, C. H., Godri, K. J., Sabaliauskas, K., and
5 Slowik, J. G. : Mass absorption cross-section of ambient black carbon aerosol in relation to
6 chemical age, *Aerosol Sci. Technol.*, 43, 522 - 532, 2009.
- 7 Lack, D. A., Langridge, J. M., Bahreini, R., Cappa, C. D., Middlebrook, A. M., and Schwarz, J. P. :
8 Brown carbon and internal mixing in biomass burning particles, *Proc. Nat. Acad. Sci. USA*,
9 109, 14802 - 14807, 2012.
- 10 Lan, Z.-J., Huang, X.-F., Yu, K.-Y., Sun, T.-L., Zeng, L.-W., and Hu, M.: Light absorption of black
11 carbon aerosol and its enhancement by mixing state in an urban atmosphere in South China,
12 *Atmos. Environ.*, 69, 118 - 123, 2013.
- 13 Lei, Y., Zhang, Q., He, K. B., and Streets, D. G.: Primary anthropogenic aerosol emission trends for
14 China, 1990–2005, *Atmos. Chem. Phys.*, 11, 931–954, doi:10.5194/acp-11-931-2011, 2011.
- 15 Lim, H.-J., and Turpin B. J. : Origins of primary and secondary organic aerosol in Atlanta: Results of
16 time-resolved measurements during the Atlanta supersite experiment, *Environ. Sci. Technol.*,
17 36, 4489–4496, 2002.
- 18 Lin, P., Hu, M., Deng, Z., Slanina, J., Han, S., Kondo, Y., Takegawa, N., Miyazaki, Y., Zhao, Y., and
19 Sugimoto N. : Seasonal and diurnal variations of organic carbon in PM_{2.5} in Beijing and the
20 estimation of secondary organic carbon, *J. Geophys. Res.*, 114, D00G11,
21 doi:10.1029/2008JD010902, 2009.
- 22 Liu, S., Aiken, A.C., Gorkowski, K., Dubey, M.K., Cappa, C.D., Williams, L.R., Herndon, S.C.,
23 Massoli, P., Fortner, E.C., Chhabra, P.S., Brooks, W.A., Onasch, T.B., Jayne, J.T., Worsnop,
24 D.R., China, S., Sharma, N., Mazzoleni, C., Xu, L., Ng, N.L., Liu, D., Allan, J.D., Lee, J.D.,
25 Fleming, Z.L., Mohr, C., Zotter, P., Szidat, S., and Prevot, A.S.H.: Enhanced light absorption
26 by mixed source black and brown carbon particles in UK winter, *Nat. Commun.*, 6, 8435,
27 2015.
- 28 Liu, X. G., Li, J., Qu, Y., Han, T., Hou, L., Gu, J., Chen, C., Yang, Y., Liu, X., Yang, T., Zhang, Y.,
29 Tian, H., and Hu, M.: Formation and evolution mechanism of regional haze: a case study in the
30 megacity Beijing, China, *Atmos. Chem. Phys.*, 13, 4501–4514, doi:10.5194/acp-13-4501-2013,
31 2013.
- 32 Lyamani, H., Olmo, F. J., and Alados-Arboledas, L.: Physical and optical properties of aerosols over
33 an urban location in Spain: seasonal and diurnal variability, *Atmos. Chem. Phys.*, 10, 239–254,
34 doi:10.5194/acp-10-239-2010, 2010.
- 35 Mack, L. A., Levin, E. J. T., Kreidenweis, S. M., Obrist, D., Moosmüller, H., Lewis, K. A., Arnott,
36 W. P., McMeeking, G. R., Sullivan, A. P., Wold, C. E., Hao, W.-M., Collett Jr., J. L., and
37 Malm, W. C.: Optical closure experiments for biomass smoke aerosols, *Atmos. Chem. Phys.*,
38 10, 9017–9026, doi:10.5194/acp-10-9017-2010, 2010.
- 39 Malm, W. C. and Hand, J. L.: An examination of the physical and optical properties of aerosols
40 collected in the IMPROVE program, *Atmos. Environ.*, 41, 3407–3427,
41 doi:10.1016/j.atmosenv.2006.12.012, 2007.
- 42 Malm, W. C., Sisler, J. F., Huffman, D., Eldred, R. A., and Cahill, T. A.: Spatial and seasonal trends
43 in particle concentration and optical extinction in the United States, *J. Geophys. Res.*, 99,
44 1347–1370, doi:10.1029/93jd02916, 1994.

- 1 Marley, N. A., Gaffney, J. S., Castro, T., Salcido, A., and Frederick, J.: Measurements of aerosol
2 absorption and scattering in the Mexico City Metropolitan Area during the MILAGRO field
3 campaign: a comparison of results from the T0 and T1 sites, *Atmos. Chem. Phys.*, 9, 189–206,
4 doi:10.5194/acp-9-189-2009, 2009.
- 5 Moise, T., Flores, J.M., and Rudich, Y.: Optical Properties of Secondary Organic Aerosols and Their
6 Changes by Chemical Processes, *Chem. Rev.*, 115, 4400 - 4439, 2015.
- 7 Nakayama, T., Sato, K., Matsumi, Y., Imamura, T., Yamazaki, A., and Uchiyama, A.: Wavelength and
8 NO_x dependent complex refractive index of SOAs generated from the photooxidation of
9 toluene, *Atmos. Chem. Phys.*, 13, 531-545, doi:10.5194/acp-13-531-2013, 2013.
- 10 Nel, A.: Atmosphere. Air pollution-related illness: effects of particles, *Science*, 308, 804–806, 2005.
- 11 Pathak, R. K., Wu, W. S., and Wang, T.: Summertime PM_{2.5} ionic species in four major cities of
12 China: nitrate formation in an ammonia-deficient atmosphere, *Atmos. Chem. Phys.*, 9,
13 1711-1722, doi:10.5194/acp-9-1711-2009, 2009.
- 14 Peng, J., Hua, M., Guo, S., Du, Z., Zheng, J., Shang, D., Zamora, M. L., Zeng, L., Shao, M., Wu,
15 Y.-S., Zheng, J., Wang, Y., Glen, C. R., Collins, D. R., Molina, M. J., and Zhang, R. : Markedly
16 enhanced absorption and direct radiative forcing of black carbon under polluted urban
17 environments, *Proc. Nat. Acad. Sci. USA*, 113, 4266-4271, doi: 10.1073/pnas.1602310113,
18 2016.
- 19 Peterson, M. R. and Richards, M. H.: Thermal-optical-transmittance analysis for organic, elemental,
20 carbonate, total carbon, and OCX₂ in PM_{2.5} by the EPA/NIOSH method, in: Proceedings,
21 Symposium on Air Quality Measurement Methods and Technology-2002, San Fran- cisco,
22 California, 13–15 November 2002, edited by: Winegar, E. D. and Tropp, R. J., Air and Waste
23 Management Association, Pittsburgh, PA, 83-1–83-19, 2002.
- 24 Pettersson, A., Lovejoy, E. R., Brock, C. A., Brown, S. S., and Ravishankara, A. R.: Measurement of
25 aerosol optical extinction at with pulsed cavity ring down spectroscopy, *J. Aerosol Sci.*, 35,
26 995–1011, 2004.
- 27 Pitchford, M., Malm, W., Schichtel, B., Kumar, N., Lowenthal, D., and Hand, J.: Revised algorithm
28 for estimating light extinction from IMPROVE particle speciation data, *J. Air Waste Manage.*,
29 57, 1326–1336, doi:10.3155/1047-3289.57.11.1326, 2007.
- 30 Quan, J. N., Tie, X., Zhang, Q., Liu, Q., Li, X., Gao, Y., and Zhao, D. L.: Characteristics of heavy
31 aerosol pollution during the 2012–2013 winter in Beijing, China, *Atmos. Environ.*, 88, 83–89,
32 doi:10.1016/j.atmosenv.2014.01.058, 2014.
- 33 Quinn, P. K., Coffman, D. J., Bates, T. S., Miller, T. L., Johnson, J. E., Voss, K., Welton, E. J., and
34 Neususs, C.: Dominant aerosol chemical components and their contribution to extinction
35 during the aerosols cruise across the Atlantic, *J. Geophys. Res.-Atmos*, 106, 20783–20809,
36 doi:10.1029/2000jd900577, 2001.
- 37 Quinn, P. K., Coffman, D. J., Bates, T. S., Miller, T. L., Johnson, J. E., Welton, E. J., Neususs, C.,
38 Miller, M., and Sheridan, P. J.: Aerosol optical properties during INDOEX 1999: means,
39 variability, and controlling factors, *J. Geophys. Res.-Atmos*, 107, 8020,
40 doi:10.1029/2000jd000037, 2002.
- 41 Quinn, P. K.: Aerosol optical properties measured on board the Ronald H. Brownduring ACEAsia as
42 a function of aerosol chemical composition and source region, *J. Geophys. Res.- Atmos*, 109,
43 D19S01, doi:10.1029/2003JD004010, 2004.
- 44 Raes, F., Bates, T., McGovern, F., and Van Liedekerke, M.: The 2nd Aerosol Characterization

- 1 Experiment (ACE-2): general overview and main results, *Tellus B*, 52, 111–125,
2 doi:10.1034/j.1600-0889.2000.00124.x, 2000.
- 3 Ramanathan, V., Crutzen, P. J., Kiehl, J. T., and Rosenfeld, D.: Aerosols, Climate and the
4 Hydrological Cycle, *Science*, 294, 2119–2124, 2001.
- 5 Ryerson, T. B., Andrews, A. E., Angevine, W. M., Bates, T. S., Brock, C. A., Cairns, B., Cohen, R.
6 C., Cooper, O. R., de Gouw, J. A., Fehsenfeld, F. C., Ferrare, R. A., Fischer, M. L., Flagan, R.
7 C., Goldstein, A. H., Hair, J. W., Hardesty, R. M., Hostetler, C. A., Jimenez, J. L., Langford, A.
8 O., McCauley, E., McKeen, S. A., Molina, L. T., Nenes, A., Oltmans, S. J., Parrish, D. D.,
9 Pederson, J. R., Pierce, R. B., Prather, K., Quinn, P. K., Seinfeld, J. H., Senff, C. J., Sorooshian,
10 A., Stutz, J., Surratt, J. D., Trainer, M., Volkamer, R., Williams, E. J., and Wofsy, S. C.: The
11 2010 California research at the nexus of air quality and climate change (CalNex) field study, *J.*
12 *Geophys. Res.*, 118, 5830–5866, doi:10.1002/Jgrd.50331, 2013.
- 13 Sun, Y. L., Wang, Z. F., Fu, P. Q., Yang, T., Jiang, Q., Dong, H. B., Li, J., and Jia, J. J.: Aerosol
14 composition, sources and processes during wintertime in Beijing, China, *Atmos. Chem. Phys.*,
15 13, 4577–4592, doi:10.5194/acp-13-4577-2013, 2013.
- 16 Sun, Y. L., Jiang, Q., Wang, Z. F., Fu, P. Q., Li, J., Yang, T., and Yin, Y.: Investigation of the
17 sources and evolution processes of severe haze pollution in Beijing in January 2013, *J.*
18 *Geophys. Res.-Atmos*, 119, 4380–4398, doi:10.1002/2014jd021641, 2014.
- 19 Sun, Y. L., Wang, Z. F., Du, W., Zhang, Q., Wang, Q. Q., Fu, P. Q., Pan, X. L., Li, J., Jayne, J., and
20 Worsnop, D. R.: Long-term real-time measurements of aerosol particle composition in Beijing,
21 China: seasonal variations, meteorological effects, and source analysis, *Atmos. Chem. Phys.*
22 *Discuss.*, 15, 14549–14591, doi:10.5194/acpd-15-14549-2015, 2015.
- 23 Takegawa, N., Miyakawa, T., Kuwata, M., Kondo, Y., Zhao, Y., Han, S., Kita, K., Miyazaki, Y.,
24 Deng, Z., Xiao, R., Hu, M., van Pinxteren, D., Herrmann, H., Hofzumahaus, A., Holland, F.,
25 Wahner, A., Blake, D. R., Sugimoto, N., and Zhu, T.: Variability of submicron aerosol
26 observed at a rural site in Beijing in the summer of 2006, *J. Geophys. Res.*, 114, D00g05,
27 doi:10.1029/2008jd010857, 2009.
- 28 Tao, J., Ho, K. F., Chen, L. G., Zhu, L. H., Han, J. L., and Xu, Z. C.: Effect of chemical composition
29 of PM_{2.5} on visibility in Guangzhou, China, 2007 spring, *Partic*, 7, 68–75,
30 doi:10.1016/j.partic.2008.11.002, 2009.
- 31 Tao, J., Zhang, L., Cao, J., Hsu, S.-C., Xia, X., Zhang, Z., Lin, Z., Cheng, T., and Zhang, R.:
32 Characterization and source apportionment of aerosol light extinction in Chengdu, southwest
33 China, *Atmos. Environ.*, 95, 552–562, doi:10.1016/j.atmosenv.2014.07.017, 2014a.
- 34 Tao, J., Zhang, L., Ho, K., Zhang, R., Lin, Z., Zhang, Z., Lin, M., Cao, J., Liu, S., and Wang, G.:
35 Impact of PM_{2.5} chemical compositions on aerosol light scattering in Guangzhou-the largest
36 megacity in South China, *Atmos. Res.*, 135, 48–58, doi:10.1016/j.atmosres.2013.08.015,
37 2014b.
- 38 Tao, J., Zhang, L. M., Gao, J., Wang, H., Chai, F. H., Wang, S. L.: Aerosol chemical composition
39 and light scattering during a winter season in Beijing, *Atmos. Environ.*, 110, 36–44,
40 doi:10.1016/j.atmosenv.2015.03.037, 2015.
- 41 Tian, M., Wang, H. B., Chen, Y., Yang, F. M., Zhang, X. H., Zou, Q., Zhang, R. Q., Ma, Y. L., and
42 He, K. B.: Characteristics of aerosol pollution during heavy haze events in Suzhou, China,
43 *Atmos. Chem. Phys. Discuss.*, 15, 33407–33443, doi:10.5194/acpd-15-33407-2015, 2015.
- 44 Tian, S. L., Pan, Y. P., and Wang, Y. S.: Size-resolved source apportionment of particulate matter in

- 1 urban Beijing during haze and non-haze episodes, *Atmos. Chem. Phys.*, 16, 1-19,
2 doi:10.5194/acp-16-1-2016, 2016.
- 3 Thompson, J. E., Hayes, P. L., Jimenez, J. L., Adachi, K., Zhang, X., Liu, J., Weber, R. J., and
4 Buseck, P. R.: Aerosol optical properties at Pasadena, CA during CalNex 2010, *Atmos.*
5 *Environ.*, 55, 190–200, doi:10.1016/j.atmosenv.2012.03.011, 2012.
- 6 Turpin, B. J. and Lim, H. J.: Species contributions to PM_{2.5} mass concentrations: revisiting common
7 assumptions for estimating organic mass, *Aerosol Sci. Tech.*, 35, 602–610,
8 doi:10.1080/02786820119445, 2001.
- 9 Varma, R., Moosmüller, H., and Arnott, W. P.: Toward an ideal integrating nephelometer, *Opt. Lett.*,
10 28, 1007–1009, 2003.
- 11 Wang, L., Li, Z., Tian, Q., Ma, Y., Zhang, F., Zhang, Y., Li, D., Li, K., and Li L.: Estimate of
12 aerosol absorbing components of black carbon, brown carbon, and dust from ground-based
13 remote sensing data of sun-sky radiometers, *J. Geophys. Res. Atmos.*, 118, 6534–6543,
14 doi:10.1002/jgrd.50356, 2013.
- 15 Wang, Q., Huang, R.-J., Cao, J., Han, Y., Wang, G., Li, G., Wang, Y., Dai, W., Zhang, R., and Zhou,
16 Y.: Mixing state of black carbon aerosol in a heavily polluted urban area of China: implications
17 for light absorption enhancement, *Aerosol Sci. Technol.*, 48, 689 - 697, 2014.
- 18 Wang, X., Huang, J., Zhang, R., Chen, B., and Bi, J.: Surface measurements of aerosol properties
19 over northwest China during ARM China 2008 deployment, *J. Geophys. Res.*, 115, D00K27,
20 doi:10.1029/2009JD013467, 2010.
- 21 Wang, X. F., Wang, T., Pathak, R. K., Hallquist, M., Gao, X. M., Nie, W., Xue, L. K., Gao, J., Gao,
22 R., Zhang, Q. Z., Wang, W. X., Wang, S. L., Chai, F. H., and Chen, Y. Z.: Size distributions of
23 aerosol sulfates and nitrates in Beijing during the 2008 Olympic Games: impacts of pollution
24 control measures and regional transport, *Adv. Atmos. Sci.*, 30, 341–353, 2013.
- 25 Wang, Y. H., Liu, Z. R., Zhang, J. K., Hu, B., Ji, D. S., Yu, Y. C., and Wang, Y. S.: Aerosol
26 physicochemical properties and implications for visibility during an intense haze episode
27 during winter in Beijing, *Atmos. Chem. Phys.*, 15, 3205–3215, doi:10.5194/acp-15-3205-2015,
28 2015.
- 29 Watson, J. G.: Visibility: science and regulation, *J. Air Waste Manage.*, 52, 628–713, 2002.
- 30 Wu, Q. Z., Wang, Z. F., Gbaguidi, A., Gao, C., Li, L. N., and Wang, W.: A numerical study of
31 contributions to air pollution in Beijing during CAREBeijing-2006, *Atmos. Chem. Phys.*, 11,
32 5997–6011, doi:10.5194/acp-11-5997-2011, 2011.
- 33 Wu, Z. J., Zheng, J., Shang, D. J., Du, Z. F., Wu, Y. S., Zeng, L. M., Wiedensohler, A., and Hu, M.:
34 Particle hygroscopicity and its link to chemical composition in the urban atmosphere of Beijing,
35 China during summertime, *Atmos. Chem. Phys. Discuss.*, 15, 11495–11524,
36 doi:10.5194/acpd-15-11495-2015, 2015.
- 37 Xu, J., Ma, J. Z., Zhang, X. L., Xu, X. B., Xu, X. F., Lin, W. L., Wang, Y., Meng, W., and Ma, Z. Q.:
38 Measurements of ozone and its precursors in Beijing during summertime: impact of urban
39 plumes on ozone pollution in downwind rural areas, *Atmos. Chem. Phys.*, 11, 12241–12252,
40 doi:10.5194/acp-11-12241-2011, 2011.
- 41 Xu, X., Zhao, W., Wang, S., Zhang, Q., Qian, X., Fang, B., Venables, D. S., Chen, W., Gao, X., and
42 Zhang, W.: Retrieval of the particulate complex refractive index by using cavity enhanced
43 aerosol albedometer, in preparation, 2016.
- 44 Yang, L. X., Wang, D. C., Cheng, S. H., Wang, Z., Zhou, Y., Zhou, X. H., and Wang, W. X.:

- 1 Influence of meteorological conditions and particulate matter on visual range impairment in
2 Jinan, China, *Sci. Total Environ.*, 383, 164–173, doi:10.1016/j.scitotenv.2007.04.042, 2007.
- 3 Yao, T., Huang, X., He, L., Hu, M., Sun, T., Xue, L., Lin, Y., Zeng, L., and Zhang, Y.: High time
4 resolution observation and statistical analysis of atmospheric light extinction properties and the
5 chemical speciation of fine particulates, *Sci. China Chem.*, 53, 1801–1808,
6 doi:10.1007/s11426-010-4006-z, 2010.
- 7 Zhang, A., Qi, Q. W., Jiang, L. L., Zhou, F., and Wang, J. F.: Population exposure to PM_{2.5} in the
8 urban area of Beijing, *PLoS One*, 8, e63486, 2013.
- 9 Zhang, H., Hu, D., Chen, J., Ye, X., Wang, X., Hao, J., Wang, L., Zhang, R., and An, Z.: Particle
10 size distribution and polycyclic aromatic hydrocarbons emissions from agricultural crop
11 residue burning, *Environ. Sci. Technol.*, 45, 5477–5482, 2011.
- 12 Zhang, X., Lin, Y. H., Surratt, J. D., and Weber, R. J.: Sources, composition and absorption
13 Angstrom exponent of light-absorbing organic components in aerosol extracts from the Los
14 Angeles Basin, *Environ. Sci. Technol.*, 47, 3685–3693, doi:10.1021/es305047b, 2013.
- 15 Zhang, Y. H., Hu, M., Zhong, L. J., Wiedensohler, A., Liu, S. C., Andreae, M. O., Wang, W., and
16 Fan, S. J.: Regional Integrated Experiments on Air Quality over Pearl River Delta 2004
17 (PRIDE-PRD2004): overview, *Atmos. Environ.*, 42, 6157–6173,
18 doi:10.1016/j.atmosenv.2008.03.025, 2008.
- 19 Zhao, W., Dong, M., Chen, W., Gu, X., Hu, C., Gao, X., Huang, W., and Zhang, W.:
20 Wavelengthresolved optical extinction measurements of aerosols using broad-band
21 cavity-enhanced absorption spectroscopy over the spectral range of 445–480 nm, *Anal. Chem.*,
22 85, 2260–2268, doi:10.1021/ac303174n, 2013.
- 23 Zhao, W., Xu, X., Dong, M., Chen, W., Gu, X., Hu, C., Huang, Y., Gao, X., Huang, W., and Zhang,
24 W.: Development of a cavity-enhanced aerosol albedometer, *Atmos. Meas. Tech.*, 7,
25 2551–2566, doi:10.5194/amt-7-2551-2014, 2014a.
- 26 Zhao, W., Xu, X., Dong, M., Chen, W., Gao, X., Huang, W., and Zhang, W.: Development of a
27 cavity-enhanced albedometer for simultaneous measurement of aerosol extinction and
28 scattering coefficients, in *imaging and applied optics 2014*, OSA Technical Digest (online)
29 (Optical Society of America), paper JTU4A.43, 2014b.
- 30 Zhao, X. J., Zhao, P. S., Xu, J., Meng, W., Pu, W. W., Dong, F., He, D., and Shi, Q. F.: Analysis of a
31 winter regional haze event and its formation mechanism in the North China Plain, *Atmos.*
32 *Chem. Phys.*, 13, 5685–5696, doi:10.5194/acp-13-5685-2013, 2013.
- 33 Zheng, G. J., Duan, F. K., Su, H., Ma, Y. L., Cheng, Y., Zheng, B., Zhang, Q., Huang, T., Kimoto, T.,
34 Chang, D., Pöschl, U., Cheng, Y. F., and He, K. B.: Exploring the severe winter haze in Beijing:
35 the impact of synoptic weather, regional transport and heterogeneous reactions, *Atmos. Chem.*
36 *Phys.*, 15, 2969–2983, doi:10.5194/acp-15-2969-2015, 2015.
- 37 Zheng, S., Pozzer, A., Cao, C. X., and Lelieveld, J.: Long-term (2001–2012) concentrations of fine
38 particulate matter (PM_{2.5}) and the impact on human health in Beijing, China, *Atmos. Chem.*
39 *Phys.*, 15, 5715–5725, doi:10.5194/acp-15-5715-2015, 2015.

40
41

1
2
3
4
5
6
7
8
9

Table 1. List of the mean optical values (aerosol extinction, scattering, absorption coefficients, and SSA at $\lambda = 470$ nm), the effective mode diameters (particle number, surface area and volume, fitted values from the measured submicron size distribution with mono-lognormal distribution function), and chemical composition of PM_{1.0} particles observed in this campaign. These parameters were classified into three different pollution levels (clear, slightly polluted and polluted days).

Parameter	Clear	Slightly Polluted	Polluted	All days	
Optical	$\alpha_{ep,470}$ (Mm ⁻¹)	58.6±81.6	186.7±161.6	567.9±292.3	200.9±239.6
	$\alpha_{sp,470}$ (Mm ⁻¹)	47.2±64.7	148.9±131.9	477.2±255.5	163.9±201.7
	$\alpha_{ap,470}$ (Mm ⁻¹)	11.6±18.3	37.8±32.3	90.9±55.8	37.0±43.2
	ω_{470}	0.81±0.10	0.79±0.07	0.84±0.06	0.80±0.08
Size	$D_{p,n}$ (nm)	38±31	73±51	120±64	67±55
	$D_{p,s}$ (nm)	374±130	338±114	335±76	351±116
	$D_{p,v}$ (nm)	478±94	480±90	455±82	475±91
Chemical Composition ($\mu\text{g}/\text{m}^3$)	OC	3.41±2.43	8.81±4.64	20.47±6.93	8.34±6.97
	EC	0.48±0.39	1.18±0.59	2.72±0.87	1.12±0.92
	NO ₃ ⁻	1.78±1.70	5.12±3.56	14.99±6.54	5.19±5.52
	SO ₄ ²⁻	1.29±0.69	3.20±2.25	9.62±4.55	3.35±3.52
	NH ₄ ⁺	0.72±0.75	2.98±2.32	9.31±4.33	2.98±3.57
	Cl ⁻	0.52±0.96	1.48±1.41	4.46±2.26	1.52±1.88
	Ca ²⁺	0.31±0.27	0.62±0.38	0.58±0.33	0.49±0.36
	K ⁺	0.16±0.25	0.50±0.38	1.18±0.46	0.46±0.48
	Na ⁺	0.19±0.22	0.33±0.28	0.60±0.38	0.32±0.30
	Mg ²⁺	0.04±0.03	0.08±0.03	0.09±0.03	0.06±0.04

10

11 Table 2. List of aerosol mean diameters and optical properties during the selected haze episode.

12

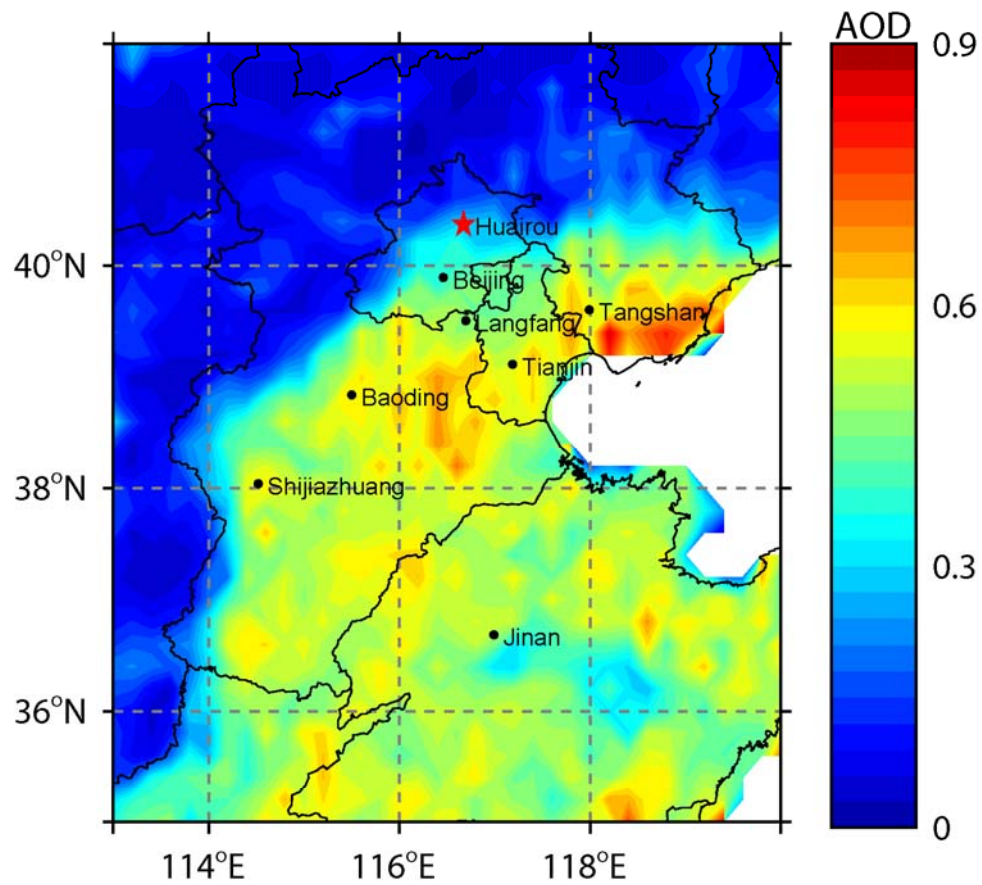
13

14

Episode	Date (LT)	Number mean diameter (nm)	Surface mean diameter (nm)	$\alpha_{ep,470}$ (Mm ⁻¹)	$\alpha_{sp,470}$ (Mm ⁻¹)	$\alpha_{ap,470}$ (Mm ⁻¹)	ω_{470}	Real part of effective CRI (n)	Imaginary part of effective CRI (k)
Period 1	22 Nov 05:40–10:00	56±6	193±19	56±24	44±19	12±6	0.79±0.03	1.38±0.06	0.03±0.02
Period 2	22 Nov 12:40–15:00	25±4	193±17	17±5	16±5	1.0±0.4	0.94±0.03	1.40±0.06	0.008±0.005
Period 3	22 Nov 15:30–23 Nov 08:00	106±16	229±16	179±69	151±57	28±12	0.85±0.01	1.39±0.04	0.02±0.006
Period 4	23 Nov 08:30–12:00	105±16	251±15	405±60	321±42	84±22	0.79±0.03	1.40±0.03	0.034±0.008
Period 5	23 Nov 12:30–24 Nov 07:30	124±19	263±11	330±110	283±94	46±16	0.86±0.01	1.44±0.03	0.02±0.01
Period 6	24 Nov 08:00–11:10	80±42	226±14	80±42	64±34	16±8	0.78±0.04	1.40±0.04	0.04±0.02

15

16

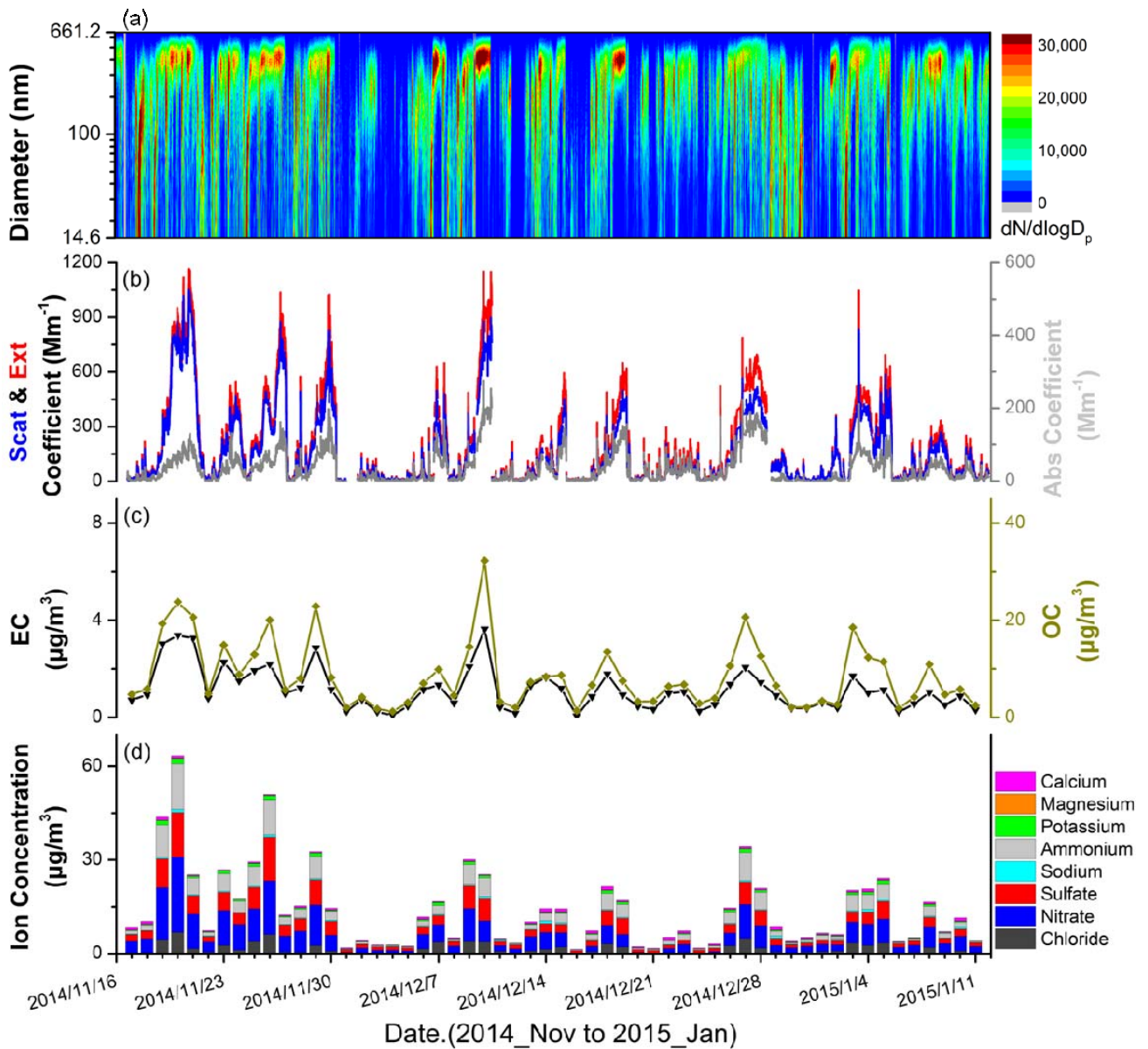


17
 18
 19
 20
 21
 22
 23
 24

Fig. 1. The map of the North China Plain. The observation site (Huairou) is marked with red star. The contour plot represents the average distribution of the MODIS AOD with $0.2^\circ \times 0.2^\circ$ resolution during the campaign (16 November 2014 to 11 January 2015).

25

26



27

28

29

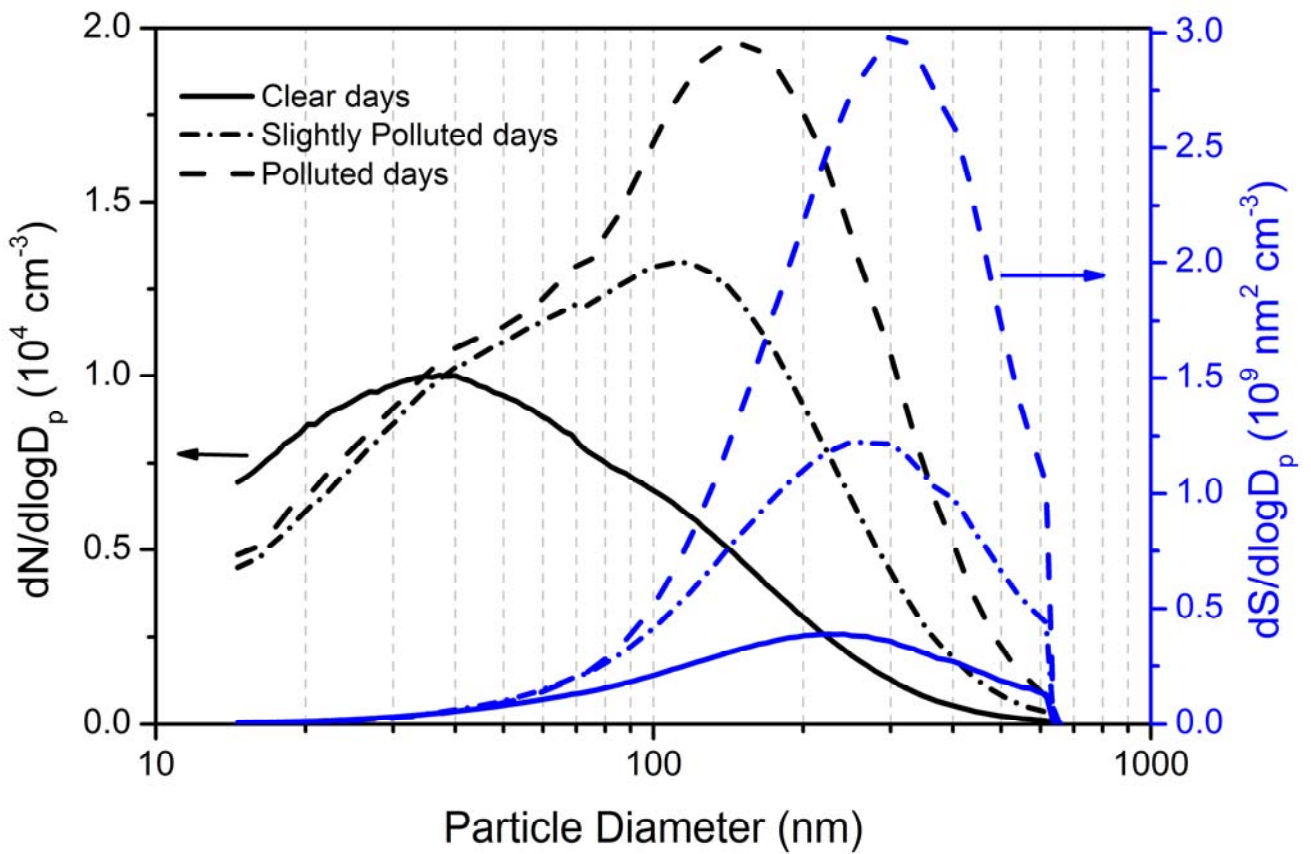
30

31 Fig. 2. Time series of (a) the aerosol number size distribution measured by SMPS, (b) the extinction,
 32 scattering and absorption coefficients at $\lambda = 470$ nm measured by cavity enhanced albedometer, (c)
 33 organic carbon and element carbon concentration measured with an off-line aerosol carbon analyzer,
 34 and (d) water-insoluble ion concentrations measured with an off-line ion chromatography of dry
 35 PM_{1.0} particles over the sampling period.

36

37

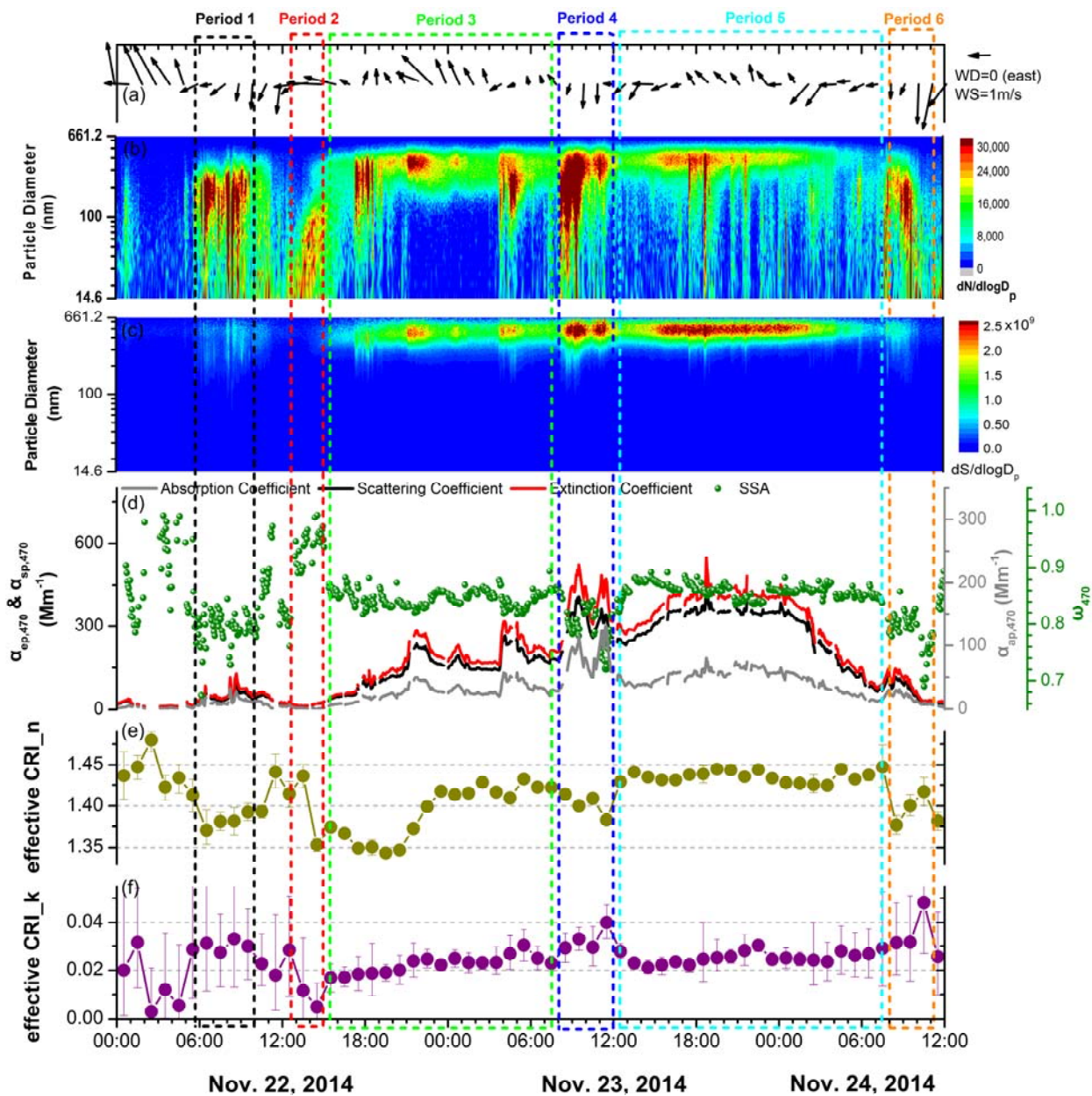
38
39
40
41
42
43
44
45
46
47



48
49
50
51
52
53
54
55
56
57

Fig. 3 The mean number and surface size distribution of ambient aerosol on clear, slightly polluted and polluted days.

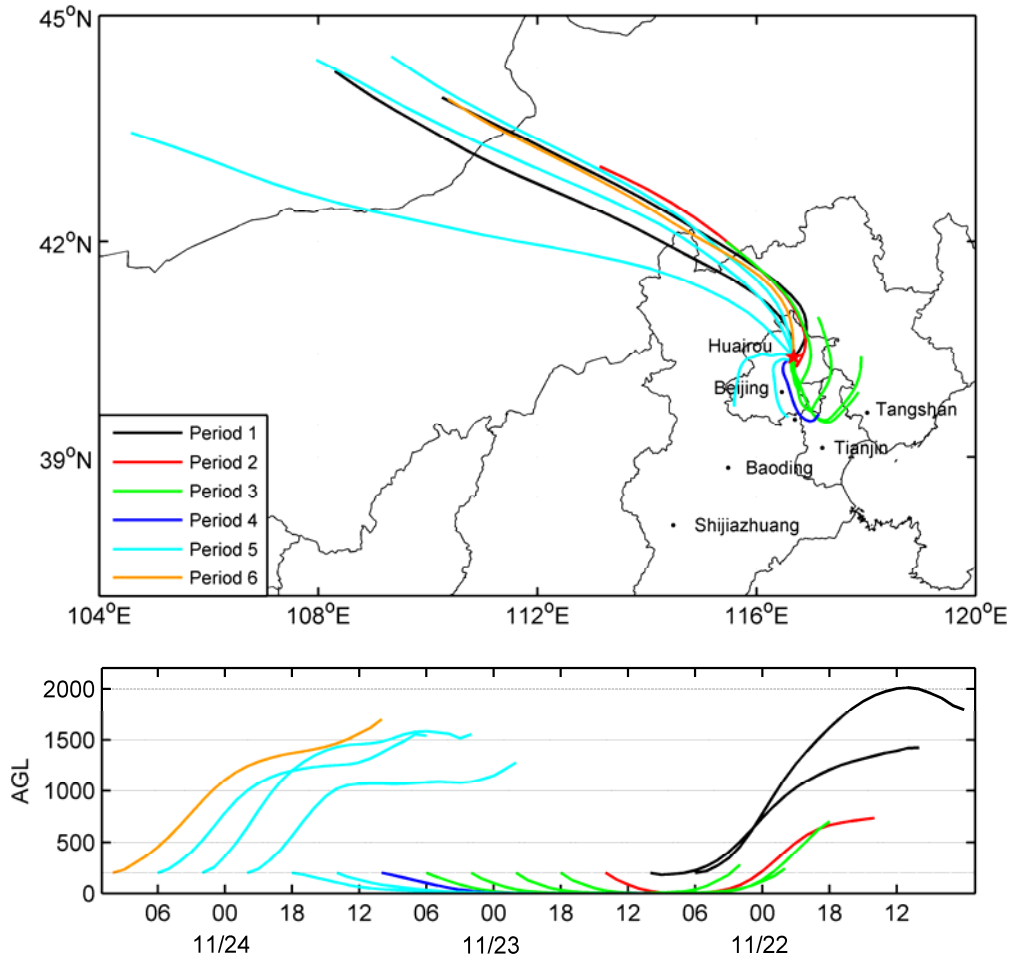
58
59



60
61
62
63
64
65
66
67
68
69
70

Fig. 4 Highly time-resolved evolution of a selected air pollution episode during November 22 to 24, 2014. (a) particle number size distribution, (b) particle surface size distribution, (c) aerosol extinction, scattering, absorption coefficients, and SSA at $\lambda = 470$ nm, (d) retrieved real part of CRI, (e) retrieved imaginary part of CRI. The air pollution episode was divided into six shorter periods to clearly show the evaluation of optical properties during haze formation, development and decline.

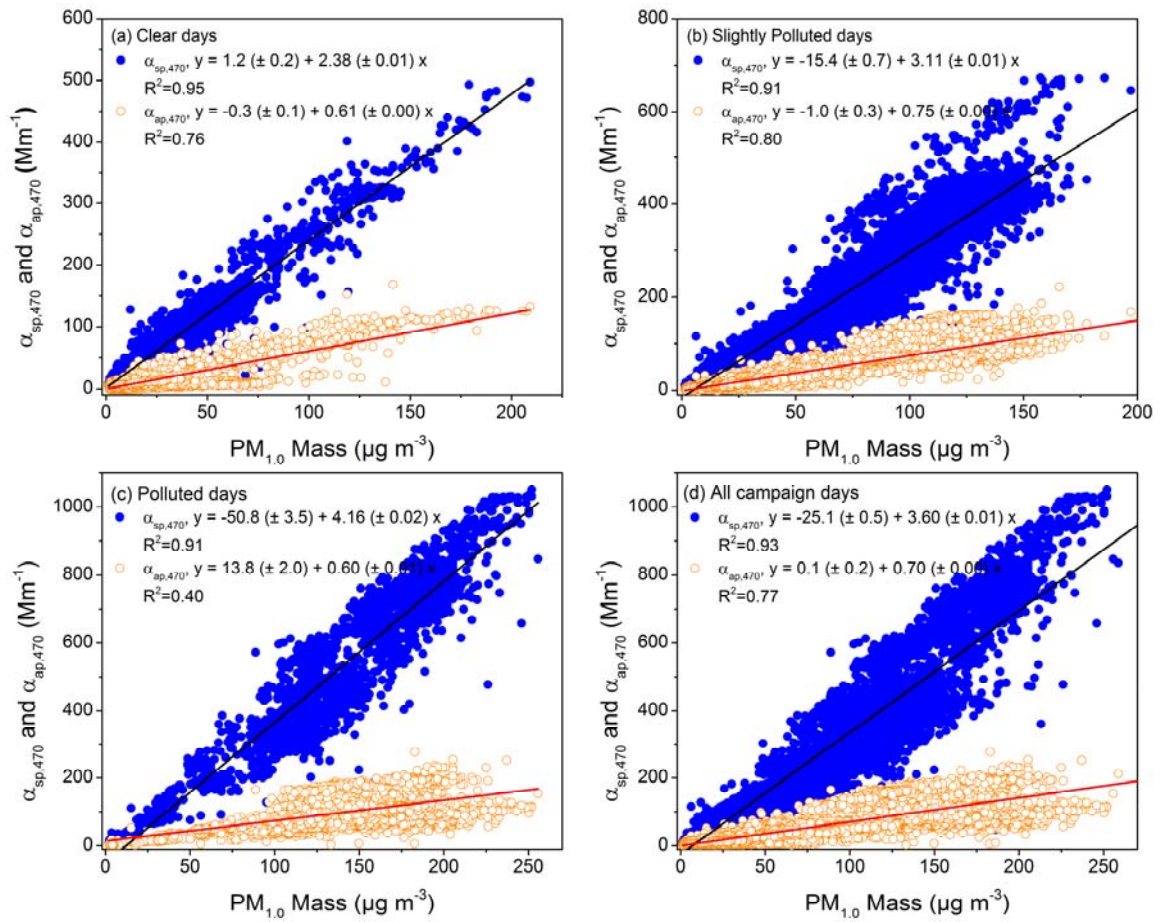
71
72
73
74



75
76
77
78
79
80
81
82
83
84

Fig. 5 The 24 hour back trajectories starting at 200 m above ground level in Huairou site were calculated every 4 h (at 00:00, 06:00, 12:00 and 18:00 local time) during the selected air pollution episode.

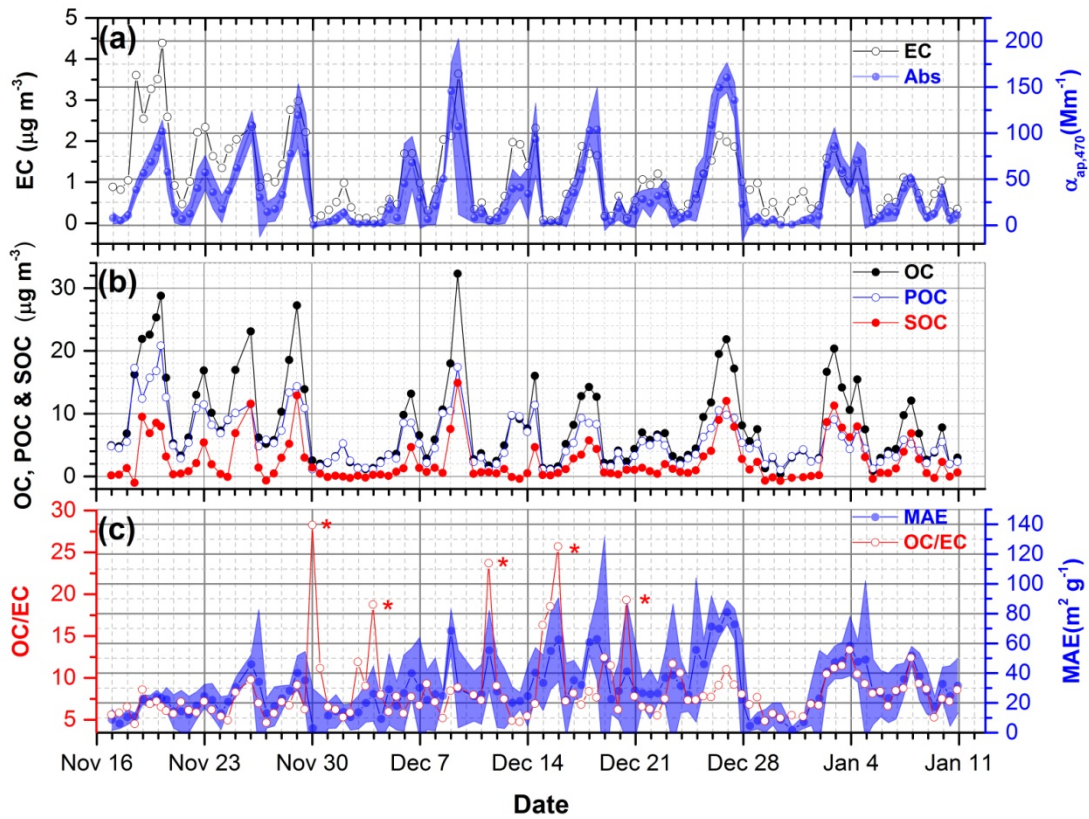
85
86
87
88
89



90
91
92
93
94
95
96
97

Fig. 6 Scatter plots of the measured scattering and absorption coefficients at $\lambda = 470$ nm against PM_{1.0} mass concentrations for PM_{1.0} particles under different pollution level.

98
99
100
101
102

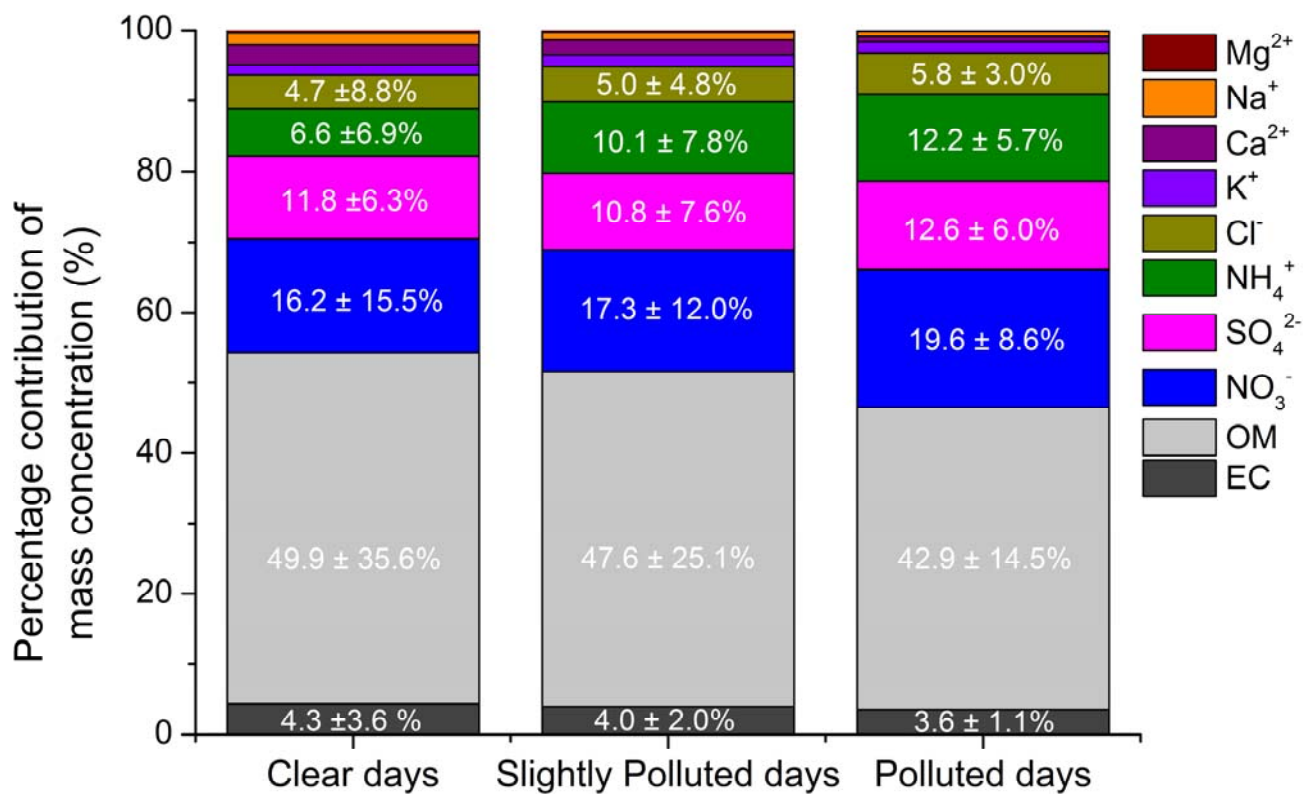


103
104
105
106
107
108

109 Fig. 7 Time series of (a) the measured EC mass concentrations and absorption coefficients at $\lambda = 470$
110 nm; (b) the measured OC mass concentrations, and the estimated primary OC (POC) and secondary
111 OC (SOC) mass concentrations determined with the EC-tracer method (Lim and Turpin, 2002; Lin et
112 al., 2009; Cheng et al., 2011, the details of the calculation method are given in the Supplement,
113 Section S7.). (c) the MAE values of EC and OC to EC ratio (OC/EC). The MAE was calculated by
114 dividing the measured absorption coefficient by the measured concentration of EC. The blue shaded
115 areas indicate the standard deviation. The red stars associated with unusually high values in (c) may
116 arised from artifacts arising from sampling or handling of the filter.

117

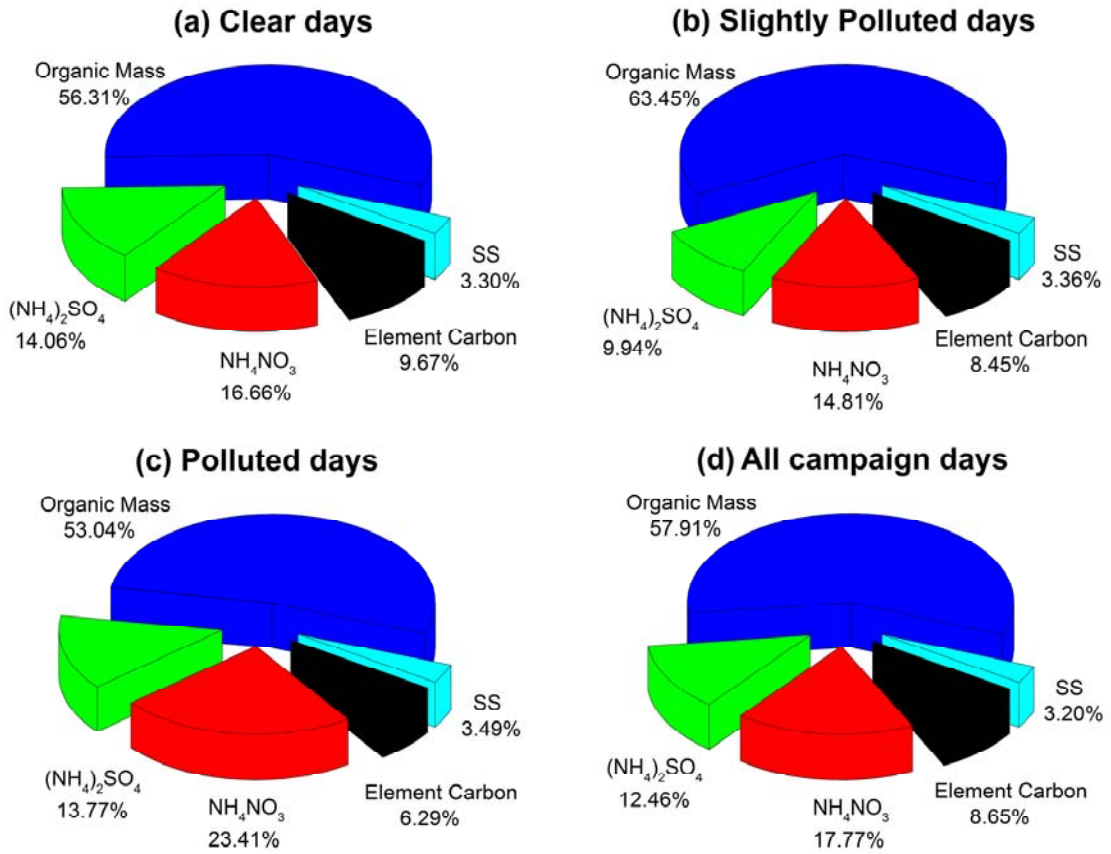
118
119
120
121
122
123



124
125
126
127
128
129
130
131
132
133
134

Fig. 8 The percentage contribution of the mass concentrations of OM, EC concentrations and eight water-soluble ion components on clear, slightly polluted and polluted days.

135
136
137
138
139



140
141
142
143
144
145
146
147
148

Fig. 9 Average fractional contribution of each chemical composition to dry $\text{PM}_{1.0}$ extinction coefficient with respect to different pollution level.